






Article

# Physical Modelling of Offshore Wind Turbine Foundations for TRL (Technology Readiness Level) Studies

Subhamoy Bhattacharya <sup>1,\*</sup>, Domenico Lombardi <sup>2</sup>, Sadra Amani <sup>1</sup>, Muhammad Aleem <sup>1</sup>, Ganga Prakhya <sup>3</sup>, Sondipon Adhikari <sup>4</sup>, Abdullahi Aliyu <sup>1</sup>, Nicholas Alexander <sup>5</sup>, Ying Wang <sup>1,6</sup>, Liang Cui <sup>1</sup>, Saleh Jalbi <sup>7</sup>, Vikram Pakrashi <sup>8</sup>, Wei Li <sup>9</sup>, Jorge Mendoza <sup>1,2</sup> and Nathan Vimalan <sup>10</sup>

- <sup>1</sup> Department of Civil and Environmental Engineering, University of Surrey, Guildford GU2 7XH, UK; sadra.amani@surrey.ac.uk (S.A.); m.aleem@surrey.ac.uk (M.A.); a.abdullahi@surrey.ac.uk (A.A.); ying.wang@surrey.ac.uk (Y.W.); l.cui@surrey.ac.uk (L.C.); j.mendozaulloa@surrey.ac.uk (J.M.)
- <sup>2</sup> Department of Mechanical, Aerospace & Civil Engineering, University of Manchester, Manchester M13 9PL, UK; domenico.lombardi@manchester.ac.uk
- <sup>3</sup> Sir Robert McAlpine Ltd., Hemel Hempstead HP2 7TR, UK; g.prakhya@srm.com
- <sup>4</sup> College of Engineering, Swansea University, Swansea SA2 8PP, UK; s.adhikari@swansea.ac.uk
- <sup>5</sup> Department of Civil Engineering, University of Bristol, Bristol BS8 1TH, UK; Nick.Alexander@bristol.ac.uk
- <sup>6</sup> School of Civil and Environmental Engineering, Harbin Institute of Technology, Shenzhen 518055, China
- <sup>7</sup> Sea and Land Projects Engineering, London SE1 1UN, UK; saleh.jalbi@seaandland.co.uk
- <sup>8</sup> School of Mechanical and Material Engineering, University College Dublin, Dublin 4, Ireland; vikram.pakrashi@ucd.ie
- <sup>9</sup> Tokyo Electric Power Services Corporation Co Ltd., Tokyo 1350062, Japan; weili@tepsc.co.jp
- <sup>10</sup> V J Tech, Reading RG2 0TB, UK; Nathan.vimalan@vjtech.co.uk
- \* Correspondence: S.Bhattacharya@surrey.ac.uk; Tel.: +44-(0)1483-689534



**Citation:** Bhattacharya, S.; Lombardi, D.; Amani, S.; Aleem, M.; Prakhya, G.; Adhikari, S.; Aliyu, A.; Alexander, N.; Wang, Y.; Cui, L.; et al. Physical Modelling of Offshore Wind Turbine Foundations for TRL (Technology Readiness Level) Studies. *J. Mar. Sci. Eng.* **2021**, *9*, 589. <https://doi.org/10.3390/jmse9060589>

Academic Editors: Eva Loukogeorgaki and Spyros A. Mavrakos

Received: 15 February 2021  
Accepted: 19 May 2021  
Published: 29 May 2021

**Publisher's Note:** MDPI stays neutral with regard to jurisdictional claims in published maps and institutional affiliations.



**Copyright:** © 2021 by the authors. Licensee MDPI, Basel, Switzerland. This article is an open access article distributed under the terms and conditions of the Creative Commons Attribution (CC BY) license (<https://creativecommons.org/licenses/by/4.0/>).

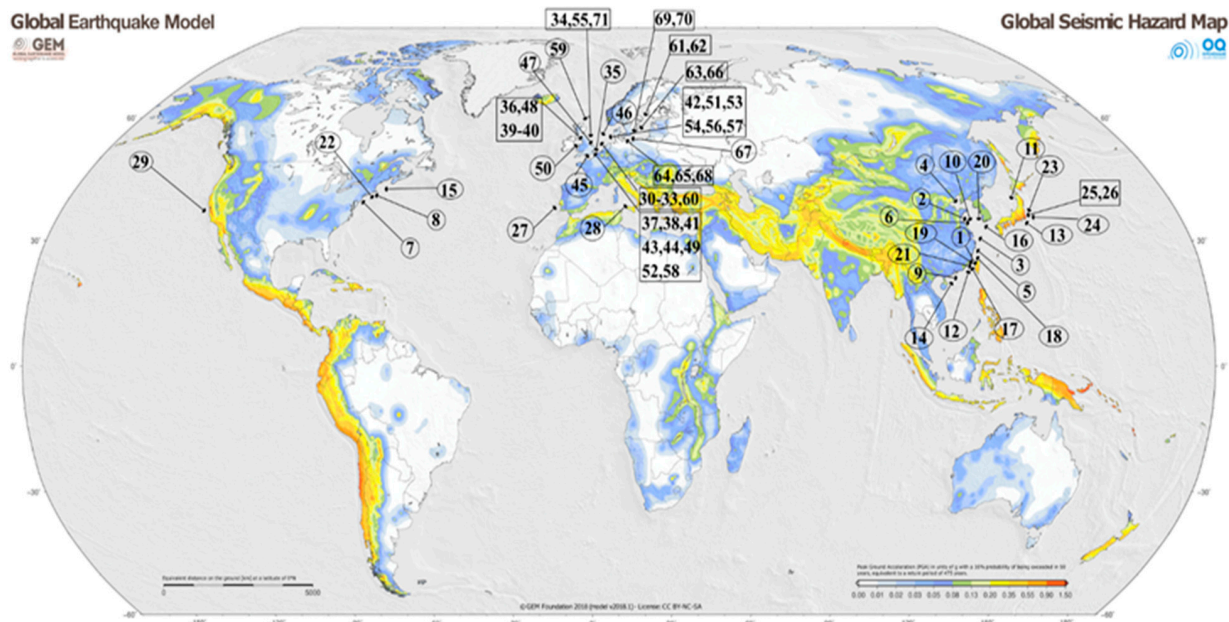
**Abstract:** Offshore wind turbines are a complex, dynamically sensitive structure due to their irregular mass and stiffness distribution, and complexity of the loading conditions they need to withstand. There are other challenges in particular locations such as typhoons, hurricanes, earthquakes, sea-bed currents, and tsunamis. Because offshore wind turbines have stringent Serviceability Limit State (SLS) requirements and need to be installed in variable and often complex ground conditions, their foundation design is challenging. Foundation design must be robust due to the enormous cost of retrofitting in a challenging environment should any problem occur during the design lifetime. Traditionally, engineers use conventional types of foundation systems, such as shallow gravity-based foundations (GBF), suction caissons, or slender piles or monopiles, based on prior experience with designing such foundations for the oil and gas industry. For offshore wind turbines, however, new types of foundations are being considered for which neither prior experience nor guidelines exist. One of the major challenges is to develop a method to de-risk the life cycle of offshore wind turbines in diverse metocean and geological conditions. The paper, therefore, has the following aims: (a) provide an overview of the complexities and the common SLS performance requirements for offshore wind turbine; (b) discuss the use of physical modelling for verification and validation of innovative design concepts, taking into account all possible angles to de-risk the project; and (c) provide examples of applications in scaled model tests.

**Keywords:** TRL (Technology Readiness Level); offshore wind turbines; scaling laws; monopile; proof of concept

## 1. Introduction

To decarbonise the energy system and combat climate change, offshore wind turbines (OWTs) are currently being constructed around the world, including in seismic areas. Figure 1 shows a seismic map with potential locations for offshore wind farms that are either operational or under development. Offshore environments present diverse metocean and geological conditions. Geological conditions include soft clay deposits in the North

Sea, chalk in the English Channel, loose sand in the South China Sea, and carbonate deposits (see Figure 2). Although existing offshore wind farms have been constructed mainly in soft clay, stiff clays, and sand deposits, future projects are likely to be deployed in more challenging geological conditions (soft rocks in shallow sea-bed, carbonate soils, and liquefiable soils) for which prior experience is limited. Foundations typically cost between 16% and 35% of a project, not only due to the challenging conditions in offshore, but also to the lack of the track record of the performance of these novel energy structures. One approach to de-risking the construction of offshore foundations is to improve the understanding of these foundations, and develop confidence in analysis and prediction using scaled model tests.



#	Wind Farm Name	Country	#	Wind Farm Name	Country	#	Wind Farm Name	Country	#	Wind Farm Name	Country	#	Wind Farm Name	Country
1	Formosa Wind Farm 1	Taiwan	15	Block Island Wind	USA	29	Redwood Coast Offshore Wind	USA	43	London Array 1	UK	60	Thornton Bank	Belgium
2	SPIC Binhai North H2	China	16	Tamra Offshore Wind Farm	Korea	30	Lely A2	Netherlands	44	London Array 2	UK	61	Karenhamn	Sweden
3	Huaneng Rudong Wind Farm (North)	China	17	Zhong Neng offshore Wind Farm	Taiwan	31	Lely A3	Netherlands	45	Rampion	UK	62	Vindpark Vanern	Sweden
4	Laotung Bodhi Offshore Wind	China	18	Formosa Wind Farm 2	Taiwan	32	Irene Vorrink	Netherlands	46	Sofia	UK	63	Avedore Holme	Denmark
5	Guodian Zhoushan Putuo 6 Offshore Wind Farm	China	19	Greater Changhua 1	Taiwan	33	Irene Vorrink	Netherlands	47	Triton knoll	UK	64	Rodsan II (Nysted II)	Denmark
6	Dongtai IV (H2)	China	20	Southwest Offshore Wind farm	Korea	34	Blyth	UK	49	Greater Gabbard	UK	65	Sprogo	Denmark
7	Skipjack wind farm	USA	21	Changfang and Xidao Wind Farm	Taiwan	35	Kentish I	UK	50	Gwynn y Mor	UK	66	Lillgrund	Sweden
8	South Fork Wind Farm	USA	22	Empire Wind	USA	36	Barrow II	UK	51	Nordsee One	Germany	67	Breitling	Germany
9	Zhuhai Jinwan Offshore Wind Farm	China	23	Choshi Wind farm	Taiwan	37	Thanet III	UK	52	Galloper	UK	68	Nysted I (Rodsan I)	Denmark
10	Jiangsu Xiangshui Offshore Wind Farm	China	24	Choshi Wind farm	Taiwan	38	Belwind	UK	53	Gemini wind farm	Netherlands	69	Middelgrunden	Denmark
11	Akita Yurihonjo offshore wind farm	Japan	25	Fukushima Floating Wind Farm (P1)	Japan	39	Burbo Bank	UK	54	Gode Wind 1 and 2	Netherlands	70	Tuno Knob	Denmark
12	Yunlin Offshore Wind Farm	Taiwan	26	Fukushima Floating Wind Farm (P2)	Japan	40	Walney I	UK	56	Nordsee Ost	Germany	71	Blyth Demonstrator	UK

Figure 1. Investments in offshore wind farm, with seismicity. The base map of the GEM model is from [1]. The data for offshore wind farms is collated from various publicly available sources.

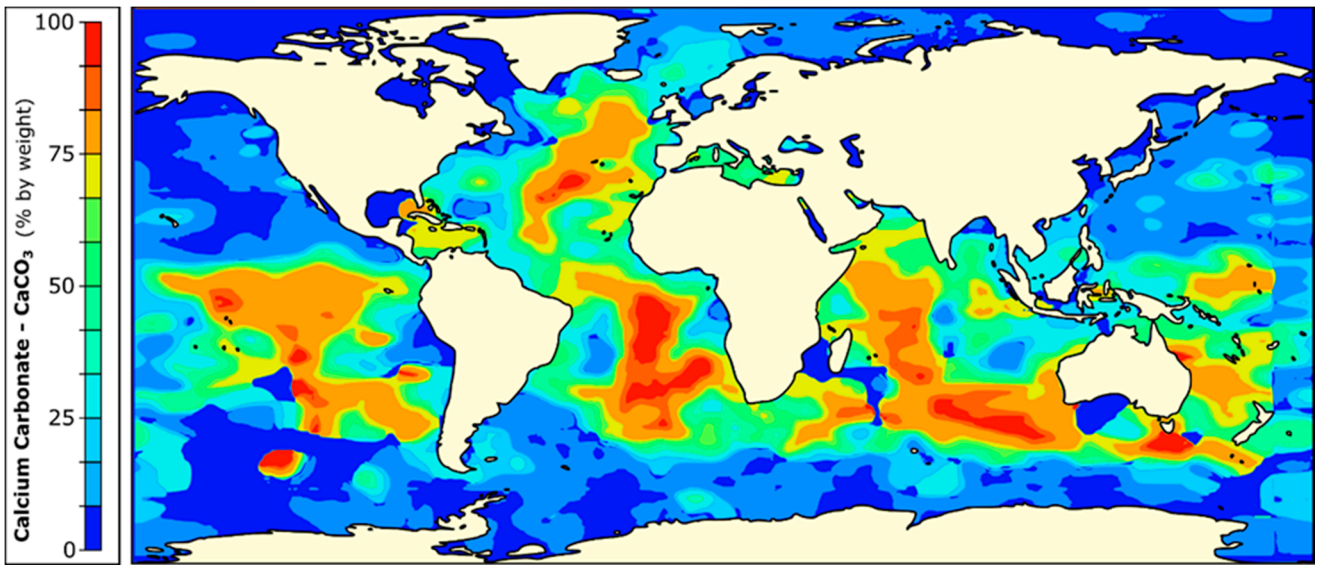


Figure 2. Carbonate sediments in offshore locations.

Figure 3 shows an inventory of foundation types for offshore wind turbines. It should be noted that although most of the operating turbines are supported on monopile foundations (these are single large-diameter steel hollow piles), future deployment farther offshore in deeper waters may require a jacket or floating structures. An overview of the type of foundations for offshore wind farms for different water depths is shown in Figure 4.

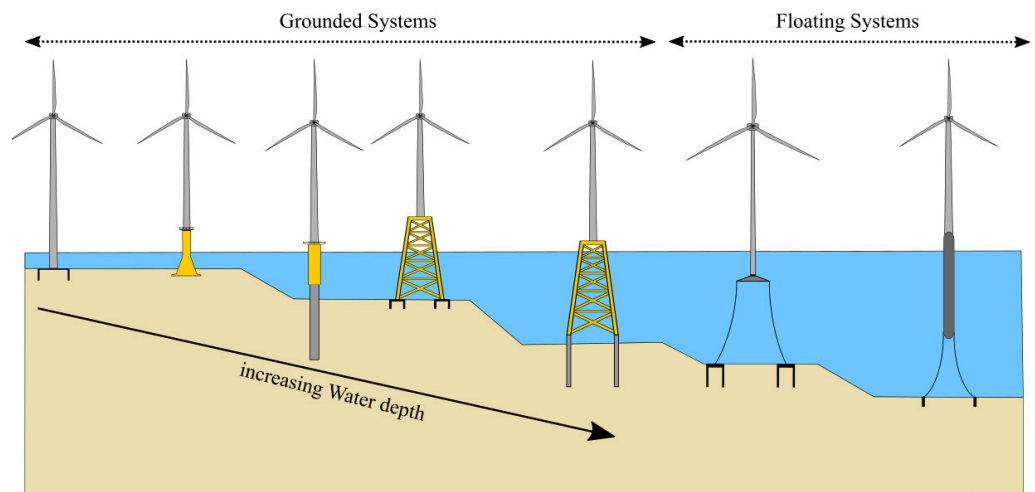


Figure 3. Commonly used foundations.

*Need for New Types of Foundations*

Offshore wind turbines are relatively new structures and differ considerably from the offshore infrastructure used in the offshore oil and gas industry. From a design perspective, one of the most important distinctions is that offshore wind turbines are extremely sensitive to dynamic loads arising from wind, waves, and earthquakes. Furthermore, they have stringent Serviceability Limit State (SLS) criteria when compared to other structures due to the presence of vibration-sensitive electrical components, notably gear boxes. The readers are referred to Chapter 3 of Bhattacharya [2] for further details. Research and development are therefore crucial to enable a significant reduction in the Levelized Cost of Energy (LCOE) and cut the subsidies on which offshore wind projects rely. One of the most promising areas of research for reducing costs is more cost-effective foundation design. Figure 5a–c shows a range of innovations that are being conceptualized to cater for challenging ground and

environmental conditions and, in some cases, to support larger turbines in deeper water. It is often useful to cite some examples, and in the context of dual challenges (both ground and loading), the example of wind farm development in China is taken. The readers are referred to [3] for such details, and here, some details are provided.

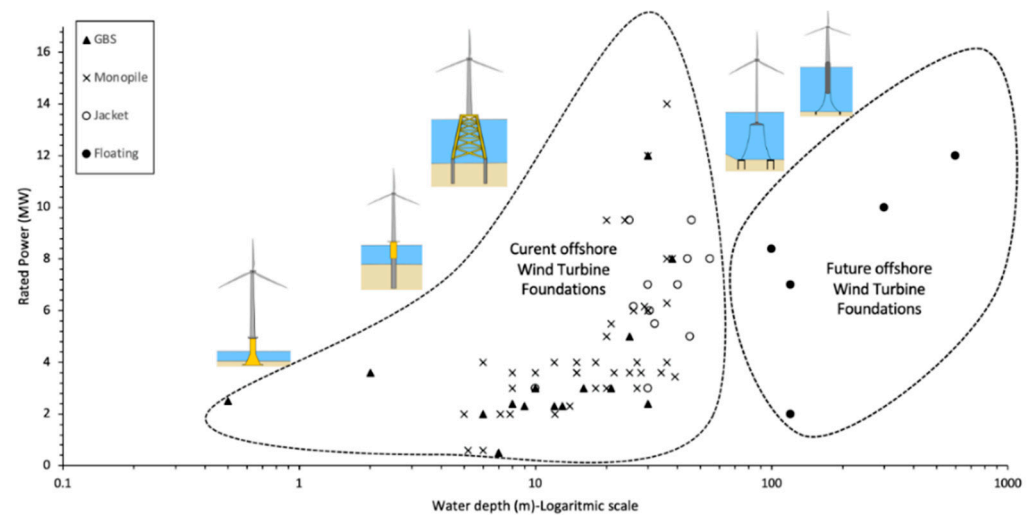


Figure 4. Proposed and existing foundation types for different water depths.

Due to the formation and deposition history, the ground in most parts of Chinese seas are soft soils interspersed with sandy silt, silty sand, and silty clay mixed with silty sand. In certain areas such as the Fujian strait, there is weathered granite at a depth of about 65 m. These regions are also subjected to typhoons where the wind speed at the hub height corresponding to a 3 s gust may exceed 70 m/s, and the average wind speed for 10 min exceeds 50 m/s. In addition to the wind speed, the maximum wave height during the peak state of the typhoon can be as high as 18 m, and the significant wave height can be 10 m with a period of between 15 and 17 s. Some parts of the Chinese seas are also subject to earthquakes which pose additional challenges. Figure 6 shows a schematic diagram of events during an earthquake: A fault rupture will generate seismic waves, which will propagate through the ground and affect the wind turbine structure. If the ground is liquefiable, it will drastically reduce the load-carrying capacity of the foundation, which may lead to excessive tilting.

**Example 1: Monopile–caisson hybrid foundation:** At the Fujian province offshore wind farm site (Putan Pinhhai Phase II) in China, engineers faced a daunting challenge of installing monopiles due to the presence of rock formations at a shallow depth. The presence of rock caused unexpected issues during monopile construction, including borehole collapse, jamming of a drilling tool, and pile tip buckling. The engineers found a solution consisting of a hybrid shallow–deep foundation, which they named monopile–caisson hybrid foundation (see Figure 5c). The main concept is that the top plate of the caisson (i.e., shallow foundation) will rest on the sea-bed, and the monopile will be fully embedded in the ground but will not touch the rock. There are no codes of practice or guidelines for such a hybrid foundation and, in these cases, scaled model tests become a necessity to validate numerical and analytical solutions.

Based on the discussion in this section, it is clear that numerous challenges are encountered when designing and constructing these foundations. A second point is that the foundations that are being used in the North Sea (European waters) cannot be automatically used in Chinese seas because they need to be evaluated against these extreme loads and ground conditions, such as typhoons, earthquakes, and soft soils. The aim of this paper is to highlight the usefulness of physical model testing, citing some examples.

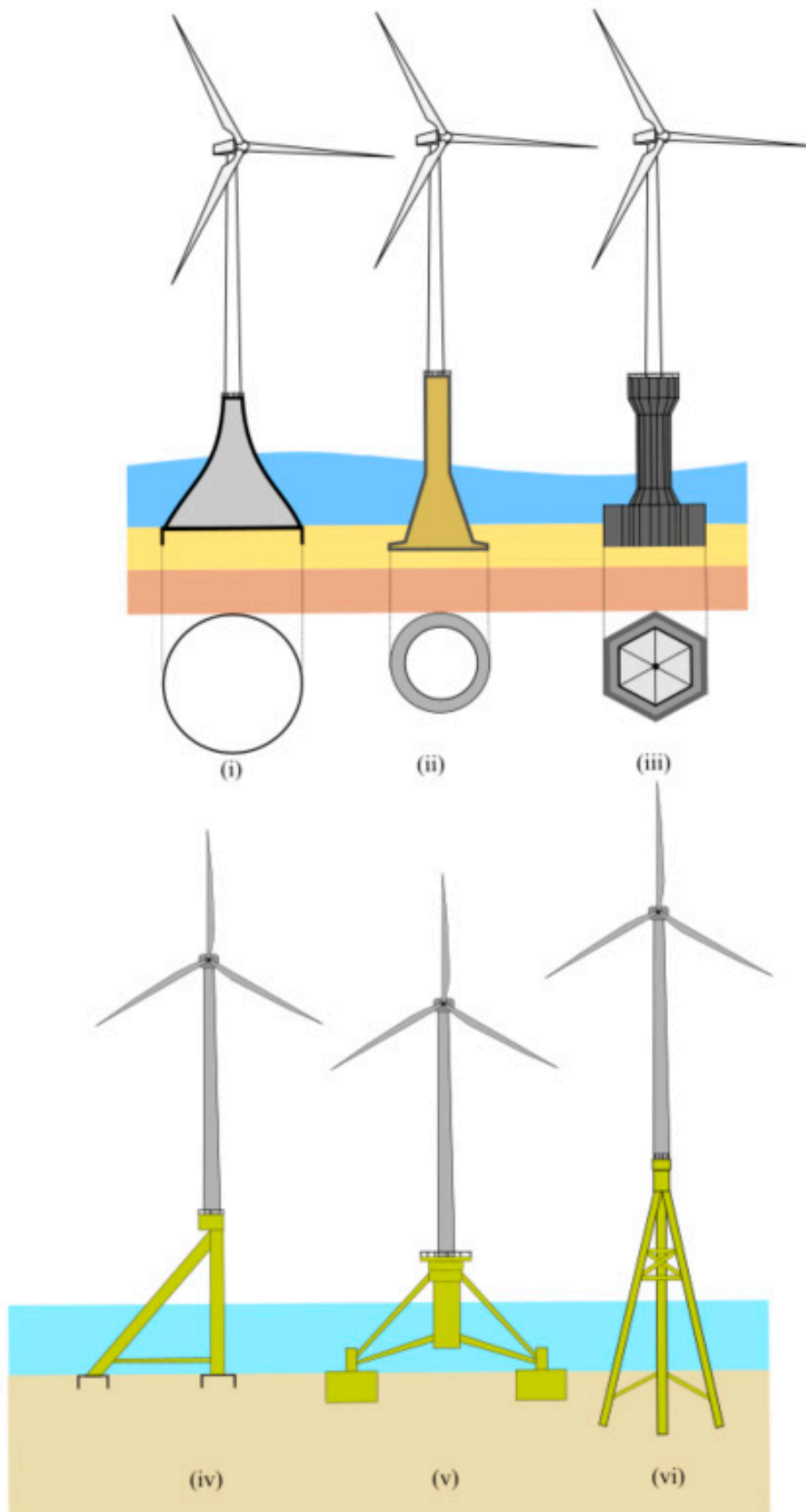
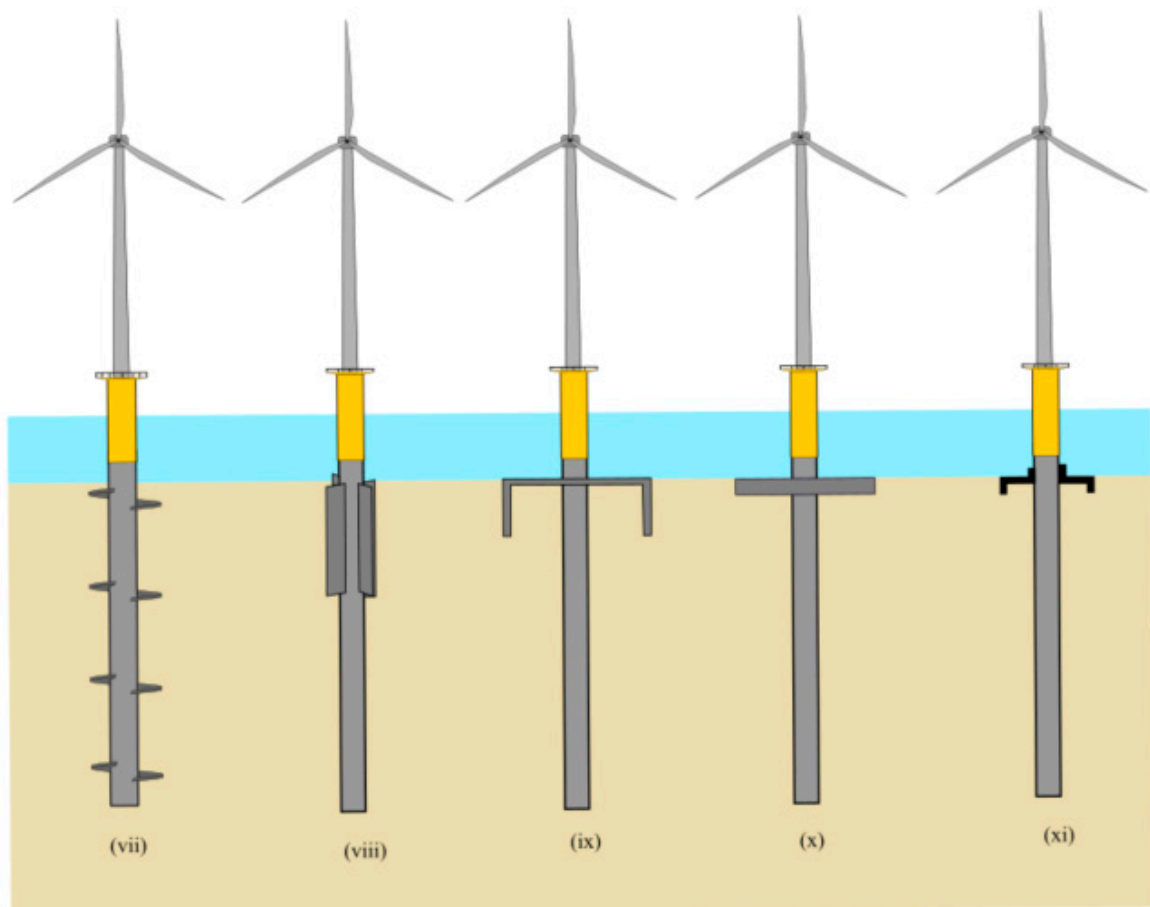
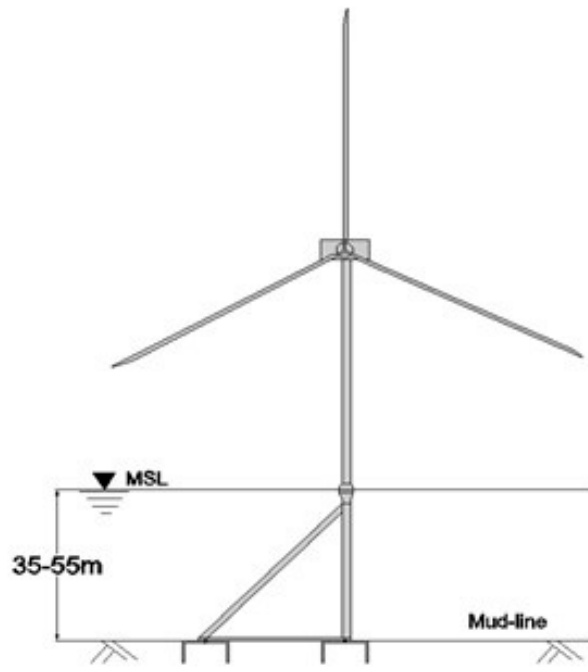


Figure 5. Cont.



(a)



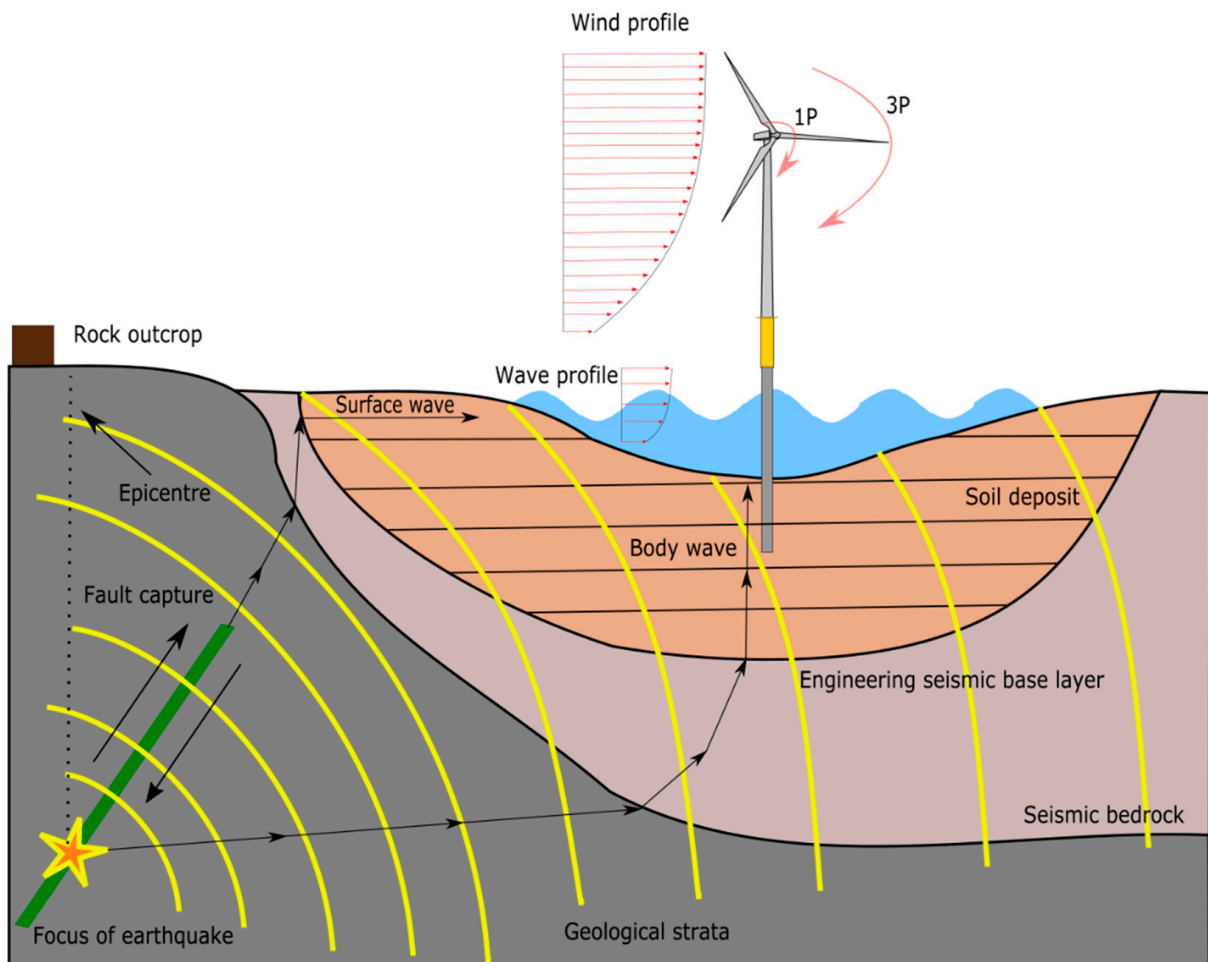
(b)

Figure 5. Cont.



(c)

**Figure 5.** (a) New foundations either in use or proposed. Some examples: gravity-based foundations (GBF) (i, ii, iii); asymmetric frame on suction caisson (iv,v see Figure 5b for more details); tetrapod/tripod on shallow foundations (iv,v); twisted jacket (vi); helical monopiles (vii); winged piles (viii); collared monopile, caisson + monopile (ix); hybrid monopile, monopile with plate (x); stiffened monopile (xi). (b) Asymmetric right-angled tripod. (c) Innovations of new foundations in China (a is a Wide Suction Bucket) and High Rise Pile Cap. Transportation of the caisson and installation of the hybrid foundation [Source: <https://www.offshore-energy.biz/first-monopile-caisson-hybrid-foundation-installed-at-chinese-offshore-wind-farm/>] (accessed date 3 February 2021).



**Figure 6.** Loading conditions for seismic locations.

## 2. Foundations for Offshore Wind Turbines: Complexity in Analysis and Design

The analysis and design of foundations for offshore wind turbines is challenging due to complex load conditions arising from the environmental loads (i.e., wind, wave, currents) and possible seismic loads in the presence of active seismic faults. Figure 7 shows a schematic diagram of the environmental loads acting on a typical offshore wind turbine, which need to be carried by the foundations and transferred to the adjacent soil. It can be seen that there are four main environmental loads, namely: wind, wave, 1P (rotor frequency) and 2P/3P (blade passing frequency), loads whose wave form is also shown in Figure 7 for a gravity-based foundation. The salient characteristics of these loads are summarized as follows:

- (a) Wind and wave result in a different offset of amplitude, frequency, and number of cycles applied to the foundation. Figure 8 shows a schematic representation of the frequency of these loads with the frequency intervals corresponding to the three possible design choices: soft–soft, soft–stiff, and stiff–stiff.
- (b) Wind and the wave loads are random in both space and time, and therefore, they are better described statistically by means of probability distributions, mean values, standard deviation, etc.
- (c) Wave and wind load act in two different directions, which give rise to the so-called wind–wave misalignment.
- (d) 1P loading is caused by mass and aerodynamic imbalances of the rotor, and the forcing frequency equals the rotational frequency of the rotor.
- (e) 2P/3P loading is caused by the blade shadowing effect, wind shear (i.e., the change in wind speed with height above the ground) and rotational sampling of turbulence. Its frequency is two or three times the 1P frequency for two and three-bladed turbines, respectively. Further details on the loading can be found in [2–5].

One of the aims of the model test is to represent these load effects appropriately in the scaled model tests. This constitutes one of the important steps in the scaled model testing [6], including aspects such as new materials [7], site-specific estimates [8], and future monitoring strategies [9]. The readers are referred to further details of physical modelling in general and its applicability in [6].

### *SLS Requirements*

The Serviceability Limit States (SLS) requirements are dictated by the intended system performance criteria. Therefore, it is necessary to discuss these criteria.

1. For a fixed wind turbine operating in a non-seismic area: The excitations due to the rotation of blades and governs the design. For such a turbine, the foundation is often allowed to rotate 0.5 to 0.75 degrees at the mudline.

2. For floating turbines in non-seismic conditions: The whole floating system stability needs to be accounted for, and the following requirements need to be addressed:

- (a) The combined pitch and roll should be within 7 to 10 degrees.
- (b) The nacelle contains critical components such as gear box, bearings and acceleration that are sensitive to acceleration. The common acceleration adopted for the design is 20% to 30% of  $g$ .
- (c) Translational displacement, also referred to as excursion, which needs to be kept within 20% of water depth.

3. For wind turbines to be operated in seismic areas, in addition to the above requirements, the following conditions need to be considered:

- (a) Possible liquefaction of loose to medium-dense sand deposits, which may induce permanent tilting to bottom-fixed foundations or loss of uplift capacity to anchors of floating systems.
- (b) Excessive vibrations due to resonance effects when the predominant frequency of the earthquake comes close to one of the fundamental frequencies of the structure.



Scaled testing for a variety of such requirements can provide guidance not only on performance but also damage; readers are referred to [10,11] for further study.

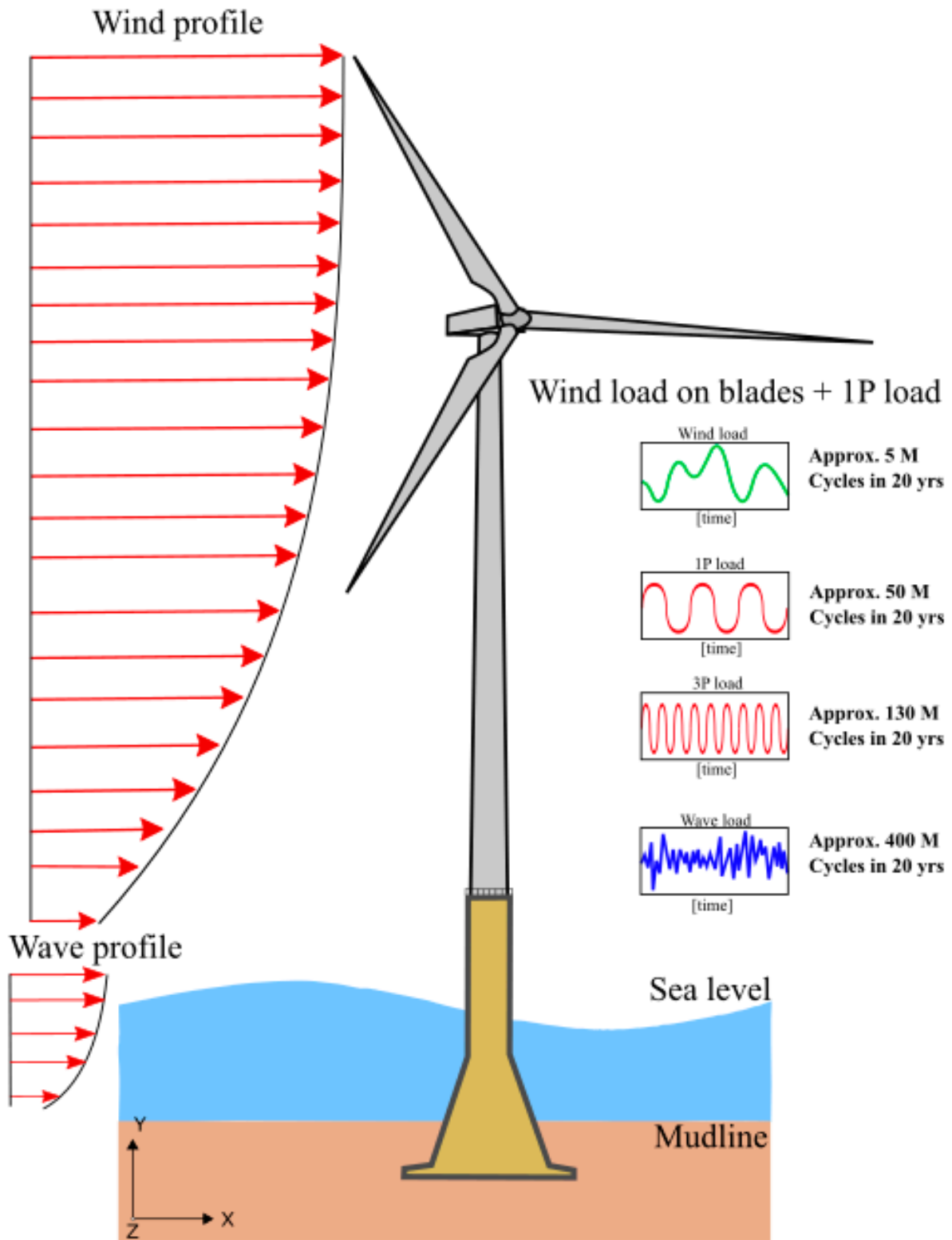


Figure 7. Load complexity with approximate number of cycles for 20 years assumed lifetime.

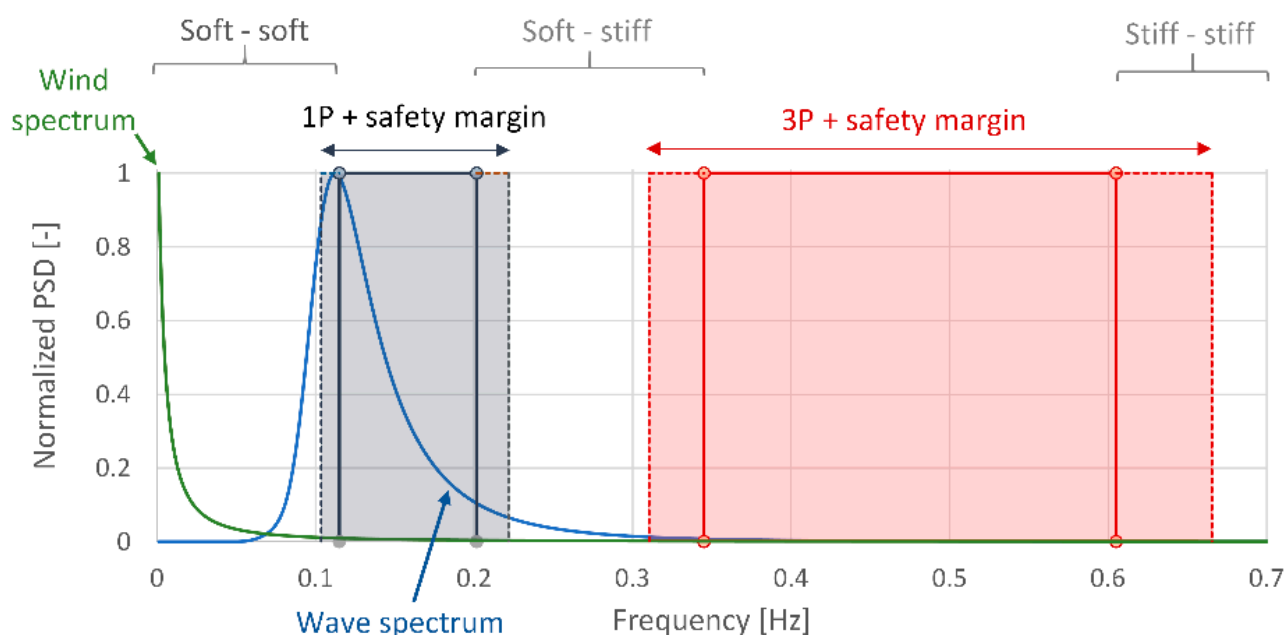


Figure 8. Design choices.

### 3. Physical Modelling in Geotechnical Engineering: A Brief Overview

The use of physical modelling in offshore and geotechnical engineering design is well established, and readers are referred to the publication [6] for further details. A non-exhaustive list of the possible use of physical modelling in offshore wind turbine application is provided below:

1. To verify the analysis/design methodologies of high-risk or novel construction techniques. For example, suction caissons are being used in North Sea grounds comprising dense sands or firm clay, and it is necessary to verify if a similar technique can be used in Chinese sites with soft soil condition. A second example is to evaluate the applicability of pressure reversal (often known as pressure cycling) to install suction caisson foundations and its effect on the post-installation uplift capacity.
2. To validate a hypothesis or a theoretical failure mode/mechanism of foundations. The example can be failure mode for a hybrid foundation (i.e., monopile with a plate (as shown in Figure 5a) or moment capacity of a screw pile. The readers are referred to the work of [12] on screw piles.
3. To recreate a failure or a collapse mechanism for settling liabilities or insurance claims.
4. To gain new insights into unexplored complex phenomena that cannot be investigated in the real field or modelled in numerical simulations due to the lack of adequately accurate soil constitutive equations. An example may include tests to investigate the cyclic behaviour of foundations in shallow gassy sediments.
5. To verify different aspects of the design for a new concept of a foundation type for which no codes of practice/guidelines or prior experience exist; that is, reducing the uncertainties in the design assumptions. Examples of particular design aspects for this specific problem of a new foundation can be modes of vibration or the modes of ultimate collapse.
6. To understand the deformations of foundations under various design situations and limit states
7. To develop design methods that may lead to the path of standardization and to validate the constitutive models of soils used in numerical models.

The need mainly arises due to the various nonlinearities (due to complex interactions involving aerodynamics, hydrodynamics, and soil–structure interaction), combined with stochasticity and uncertainties (due to design parameters such as those of the soil and

long-term loading conditions and issues such as biofouling) of the problem in hand, which occur at various timescales. It is important to note that soil is a broad class of materials that have been produced by various natural geophysical and biological processes over millennia. Soil is multiphase and essentially an assembly of heterogeneous particulate material components, and its averaged constitutive characteristics are non-linear and dependent on strain amplitude and loading path. It is often characterized by macroscopic (averaged) parameters, such as strength, stiffness, and permeability.

Physical modelling provides a vital tool for gaining insights into some of the complex phenomena and soil–structure interaction occurring within the soil, including intervention options such as control [13–16]. Therefore, testing a large number of physical models is necessary as an alternative to full-scale tests, which are too expensive to justify. Readers are referred to PISA-based projects, which are near full-scale; see reference [17]. Thus, it becomes readily apparent that a scaling-down of the test model is required. However, the question remains how does one design a scaled model such that its results give credible insight into the behaviour of the full-scale prototype geotechnical structure? Due to the sharp increase in the use of floating turbines, methods relating to these scaled tests [18,19] are becoming increasingly important. As a result, better clarity around this topic will not only benefit the evolving offshore wind sector but also the burgeoning ideas relating to the wave device sector [20,21].

#### 4. Physical Modelling of Offshore Wind Turbine Foundations

Before any new type of foundations can be deployed for real offshore wind farm projects (see Figure 5), a thorough technology review needs to be carried out to de-risk the project. Moreover, validation of new foundation types through testing is the requirement of certifiers such as DNV-GL and Lloyd’s Register. The European Commission defines this process through the so-called Technology Readiness Level (TRL), whose steps are briefly summarized in Table 1.

**Table 1.** Technology Readiness Level (TRL).

TRL Level as European Commission	Interpretation of the Terminology and Remarks
TRL-1: Basic principles verified	It is necessary to verify that the governing mechanics principles are obeyed. For example, in the case of foundations, it must be checked whether the whole system is in equilibrium under the action of environmental loads.
TRL-2: Technology concept formulated	It is necessary to assess the whole technology starting from fabrication to methods of installation, and operation and maintenance (O&M), and decommissioning. In this step, it is expected that method statements will be developed.
TRL-3: Experimental proof of concept	Small-scale models need to be tested to verify steps in TRL-1 and TRL-2. In terms of foundation, this would correspond to checking the modes of failure in Ultimate Limit State (ULS) and identifying the modes of vibration.
TRL-4: Technology validated in lab	Once TRL-3 is satisfied and the business decision is taken to go ahead with the development/design, it is necessary to determine that the proposed technology is sound under the most likely scenarios encountered during the operation of the wind turbine. This may include long-term performance under millions of cycles of loading and evaluate the dynamic performance over the lifetime in relation to Serviceability Limit State (SLS) Fatigue Limit State (FLS).

Table 1. Cont.

TRL Level as European Commission	Interpretation of the Terminology and Remarks
TRL-5 Technology validated in relevant environment	Validation in a relevant environment may require further numerical simulation in which models are calibrated based on the results from the small-scale model tests and element tests. In the context of foundation, this step may use advanced soil constitutive models to verify the performance under extreme loading.
TRL-6: Technology demonstrated in relevant environment	To demonstrate the technology in the relevant environment, a prototype foundation may need to be constructed and tested in the offshore environment representative of the real site conditions.
TRL-7: System prototype demonstration in operational environment	The foundation is subjected to operational loads, and the performance is monitored.
TRL-8: System complete and qualified	Based on the results in TRL-7, the system can be classified as qualified or not qualified, or changes are required.
TRL-9: Actual system proven in operational environment	Technology may be used in energy generation with contingency plans.

Figure 9 shows an example of TRL-1 (i.e., checking of basic principles) for a tetrapod foundation whereby the load transfer from the structure to the ground is shown. By comparison, one of the early studies that must be carried out is technology validation in the laboratory environment (TRL-3 and -4); in this context of foundations, this would mean carrying out tests to verify the possible failure mechanisms, modes of vibration, and long-term performance under the action of complex and repetitive loads. It must be realized that it is very expensive and operationally challenging to validate the new technology in a relevant environment, and therefore laboratory-based testing may offer a more economical solution that is robust enough to justify the next stages of investment.

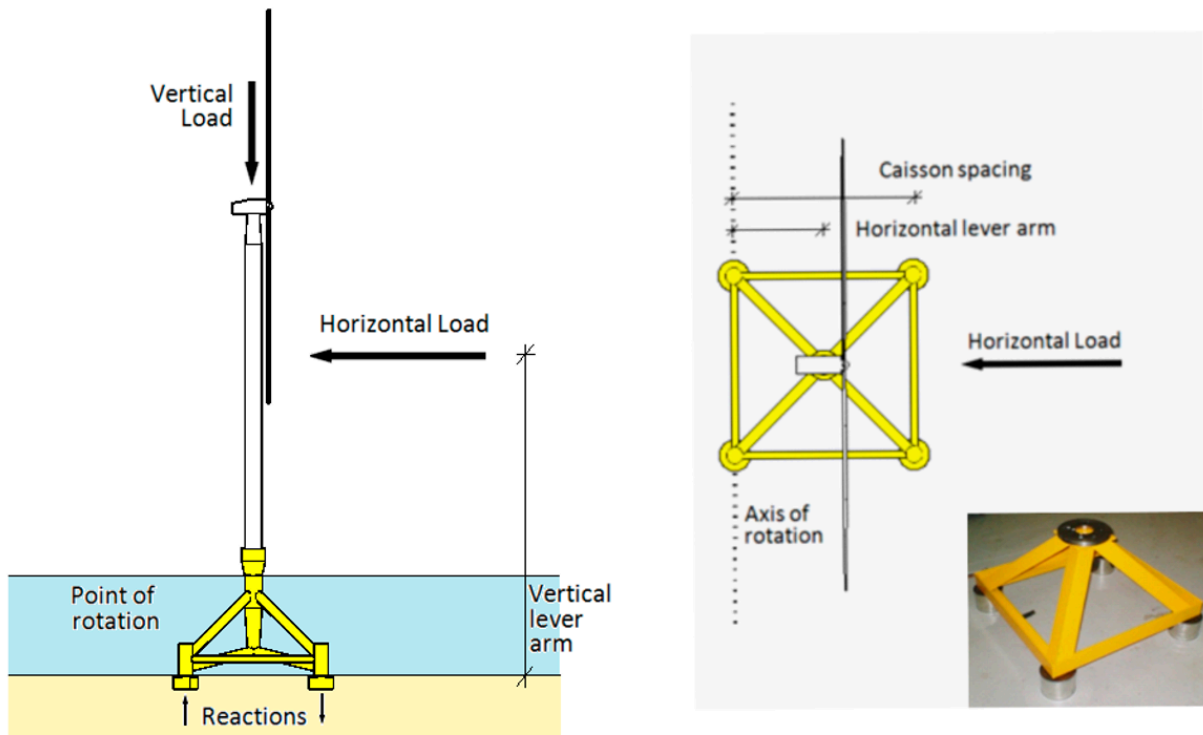


Figure 9. Example of TRL-1 type studies for tetrapod foundation.

#### 4.1. Requirements of Foundation Testing for Offshore Wind Turbine Foundations

The design requirements stem from the performance necessary and is mostly guided by turbine manufacturer performance specification because the main objective is to maximize the energy output over the lifetime. For foundation design, the main issues are as follows:

- (i) Load transfer from the superstructure to the supporting ground in the case of extreme load events.
- (ii) Modes of vibration of the adopted structural system, i.e., rigid rocking modes or flexible modes or a combination.
- (iii) Long-term change in dynamic characteristics, i.e., change in natural frequency and damping due to repetitive cyclic loads or extreme dynamic loads associated with natural hazards such as typhoons and earthquakes.
- (iv) Long-term deformation does not violate stringent SLS requirements, such as being limited to maximum rotation.

#### 4.2. Suitability on Different Methods of Testing

Behavior of offshore wind turbines involves complex dynamic wind–wave–foundation–structure interaction, and the control system onboard the RNA hub adds further interaction. There are different established methodologies for testing the main critical components, including:

- (a) Wind tunnel testing can model the aerodynamics and aeroelasticity interaction, and the performance of the blades.
- (b) Wave tanks can be used to model hydrodynamic issues, including tsunami loads.
- (c) Geotechnical centrifuge testing can model soil–structure interactions with correct stress–strain behaviors.
- (d) A shaking table at 1 g or in a geotechnical centrifuge can model the seismic performance, including dynamic soil–structure interaction (DSSI).

In wind tunnel tests, aerodynamic effects are modelled efficiently and correctly, and as a result, the loads on the blade and towers can be simulated. By comparison, in a wave tank, the hydrodynamic loads on the sub-structure and scouring on the foundation can be modelled. In a geotechnical centrifuge, one can model the stress level in the soil, but the model package is spun at a high RPM which will cause unwanted vibrations in the small-scale model. Ideally, a tiny wind tunnel together with a tiny wave tank onboard a geotechnical centrifuge may serve the purpose, but this is not viable and will add more uncertainty to the models than it tries to unearth. Each of the techniques has its own limitations, and these aspects must be taken into consideration when scaling the observations. Therefore, the focus of the experiments needs to be on the governing laws or mechanics or process.

A model need not be more complex than necessary, and often simple experiments can unearth the governing laws. In every type of experiment, there will be cases where the scaling laws/similitude relationships will not be satisfied (rather, they will be violated), and these must be recognized when analyzing the test results. Therefore, results of scale model tests for offshore wind turbine problems involving so many interactions (examples include aerodynamics, hydrodynamics, damping from three different mediums—air, water and soil, control system intervention affecting misalignment of wind and wave) should not be extrapolated for prototype prediction through scaling factors ( $N^a$ , where  $N$  is typically the geometrical scale ratio and  $a$  is the scaling factor). Damping is complex and often dictates the response; readers are referred to [22] for a detailed and comprehensive account of damping. Furthermore, Adhikari and Bhattacharya [23] recently proposed a physics-based mechanical model on damping of the whole system. Within a dynamic stiffness framework, it was shown that there are seven unique damping coefficients that quantify the damped response of wind turbines.

Therefore, tests must be carried out to identify trends of behaviour and better understand the main governing mechanisms. Upscaling must be carried out through laws of physics that are understood from these tests, using numerical/analytical models and linked to readily available soil-element tests (e.g., triaxial tests and resonant columns). In this case, the uncertainties are reduced as the designer used realistic soil parameters and employed the physics of the problem. Figure 10 shows the usefulness of small-scale tests and its application in developing design methods. A summary of the salient points discussed above can be found in Table 2.

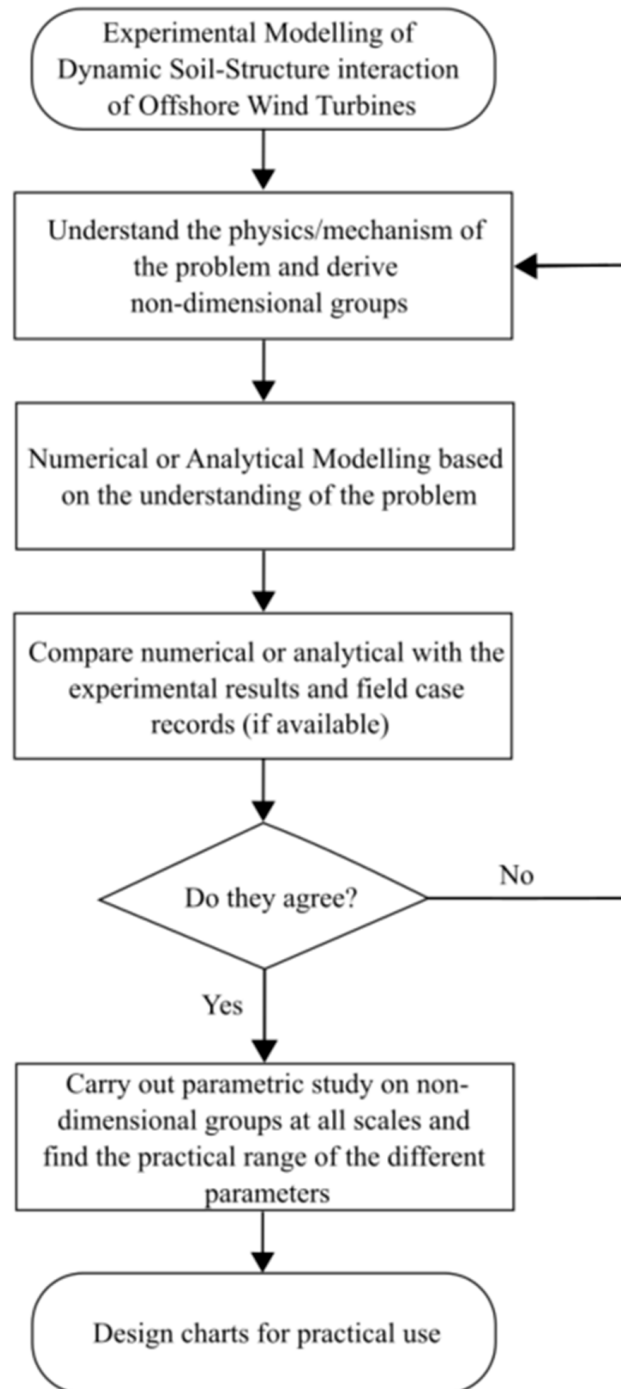


Figure 10. Flowchart showing the usefulness of scaled laboratory testing (Bhattacharya, 2019).

**Table 2.** Different forms of testing for offshore wind turbines.

Types of Testing	Remarks on the Understanding
Wind Tunnel testing	Blades can be tested to show the importance of profile.
Wave Tank Testing	Wave tank of different forms can be used to study scour, hydrodynamic loading, tsunami.
Geotechnical Centrifuge	Geotechnical centrifuge enables replication of the stress levels that the soil experiences in the field. However, the whole model is spun at a high rate which creates unwanted small vibrations. Therefore, the subtle dynamics of the problem is difficult to study as filtering of signals are inevitable during the processing of data.
Whole System modelling	Small-scale whole system modelling, which can be considered as a full-scale prototype pioneered by [24], is one approach to studying the overall system. This type of modelling was used to carry out TRL of a Self-Installing Wind Turbine (SIWT) asymmetric tripod; details are provided in [25]. Because the system is tested on a stable floor, dynamics of the problem can be readily studied. Further details can be found in [6].

#### 4.3. STEPS in Designing Scaled Mode Tests

Bhattacharya et al. [6] proposed the necessary steps in designing meaningful scaled model tests, which can be summarised as follows:

**STEP 1:** Identify the potential failure mechanisms or processes that are likely to occur, i.e., the aims and objectives of the testing program. Care needs to be taken for the cases in which a priori assumptions preclude certain system behaviour of potential interest in the prototype. Using the example of offshore wind turbine, one vital aspect is the modes of vibrations. Which mode or modes are important to use for similitude scaling laws? For example: Do we assume the flexible tower is coupled with an equivalent rocking foundation soil spring? Or do we neglect the soil rocking foundation soil spring (in our similitude laws) by assuming the foundation is just too rigid? This step is physics or mechanics based.

**STEP 2:** Deduction of the relevant non-dimensional groups for the identified mechanisms or processes in Step 1. Numerous approaches can be used: (a) analytically through the approximate governing equations and then using non-dimensional procedure; and (b) Buckingham Pi theorem [24] without the need of deriving the approximate governing equations explicitly. This step is mathematics based, and often finite element analysis (FEA) may be used as a sanity check of the analytical solutions.

**STEP 3:** Ensure that the set of crucial scaling laws (which are essential) are simultaneously conserved between model and prototype through pertinent similitude relationships.

**STEP 4:** Identify scaling laws that are approximately satisfied, and those which are violated and therefore require special consideration. Examples of the latter are stiffness and dilatancy of soils in 1 g testing, and small amplitude vibration monitoring and damping in centrifuge modelling.

Once the non-dimensional groups are identified, scaled tests need to be designed to check the nonlinearity amongst those groups and compare with numerical results where applicable. These non-dimensional groups can later be used to develop design charts. Scaling or developing constitutive relations is one of the challenging steps in a successful scaled test. If the scaling for a particular problem is incorrect, the experiment carried out will not show the dominant mechanism. It is important to use an example to highlight this critical point.

**Example 2:** The example of slender piles in liquefiable soils is taken. The relevance of this example is that wind turbine jackets in liquefiable soils will be supported on slender piles: Piles in seismically liquefiable areas are often long and slender (length to diameter ratio as high as 100) and they carry a large axial load. If the physical modelling of the

collapse of pile-supported structures during the earthquake was conducted with no axial load (or pile head mass), the buckling instability mechanism of slender piles would not be invoked. An example of dimensional analysis for piles in liquefiable soils can be found in [26]. Therefore, identification of the correct mechanism is necessary for the right scaling.

It may often be argued that experiments must be conducted if the mechanism is to be understood. The issue in hand is analogous to that of the chicken or the egg, or a catch-22 situation; that is, which comes first? This highlights that scaled experimentation in relation to understanding is an iterative process. It is clearly necessary to conduct more than one type of scaled test, and an iterative loop and analytical models to explore parametric configurations.

Bhattacharya [6] suggested a foolproof method as follows:

- (a) List all of the failure mechanisms (however improbable they are) and then rank them. Write down the governing equations based on simple mathematical idealization. In this context, readers are referred to the work of Adhikari and Bhattacharya [23,27] on the non-dimensionalization of the Euler–Bernoulli equation considering the flexibility of the foundation.
- (b) Carry out finite element analysis of the same problem as a sanity check because not all of the parameters can be accounted for in the simple idealistic analysis.
- (c) Following the above two steps, scaling and derivation of the similitude relationships can be undertaken. Then, the experiments can be designed and carried out.
- (d) Verify if the experiments show the predicted behavior. Subsequent rounds of experimentation may be required depending on the outcome. New lessons may be learnt that were previously thought to be unimportant, and vice versa.
- (e) Iterate the above procedure until the convergence of understanding.

In complex interaction problems, the use of mechanics-based scaling laws is crucial for the interpretation of the results, as opposed to black-box type scaling laws. Several examples of an offshore wind turbine are taken to illustrate the point. As explained in the previous section, offshore wind turbines are complex systems with uncertain material behavior (ground supporting the foundation), aero–hydro–servo dynamic soil–structure interactions. As a result, large non-linearities are possible.

Certain guidelines exist in physical modelling when dealing with complex interaction problems:

#### **DO**

1. It is important to replicate the mechanisms (for example, failure mechanism) in small-scale tests. This is shown below using the example of the failure of an anchor foundation for floating wind turbines, i.e., the verification of Ultimate Limit State (ULS) design.
2. Each test needs to be repeated at several scales (at least three), such as 1:200, 1:100, and 1:50. This is often termed “Modelling of models” in the literature to remove artefacts (if any) and to establish reliability. Nonlinearity is defined by amplitude, and this step helps to identify non-linear behaviour. It is shown below that two peak modes of vibration were identified for turbines supported on multiple shallow foundations.
3. Physical mechanisms or processes (essentially the laws of physics) must be identified that govern the observation or control the behavior of interest. This can guide Serviceability Limit State (SLS).
4. If possible, the governing equation should be written and, using mathematical techniques, the non-dimensional groups should be identified.
5. Check nonlinearity of the non-dimensional groups.

#### **DO NOT**

1. Unless it is a very simple problem, do not scale the numerical values of the observations to predict the prototype consequences. There is often a tendency to use standard charts and scale the observations.



### 5. Mechanisms to Be Considered in Scaled Modelling for Offshore Wind Turbine Foundations

This section of the paper highlights some of the soil–structure interactions (SSI) due to cyclic and dynamic loading on the foundation. Figure 7 shows a schematic diagram showing the four main loadings on a wind turbine. Figure 11 shows a time history of the overturning moment at the foundation level caused by wind and wave loads. It can be seen that the wind and waves provide the largest overturning moment on the foundation, which is typically three orders of magnitude higher than that induced by the blade rotation through 1P and 3P frequencies. As a result, effects due to blade rotation may be neglected when designing scaled model tests for physical modelling. Jalbi et al. [28] confirmed that the bending moment time history in Figure 11 compares well with results from the simulation in aero-elastic code. Further details of the loading, including the methods to estimate the overturning moments on the foundation, can be found in [4,29]. Furthermore, these showed that wind-induced excitation produces the largest cyclic lateral load (and cyclic overturning moment) at the foundation level. It should be noted that due to the low forcing frequency of wind loading, the resulting cyclic lateral load does not (typically) contribute dynamic effects, such as resonance; however, this is important for fatigue analysis. In contrast, wave, 1P and 3P loading will produce dynamic loading on the foundation due to the proximity of frequency of these loads to the natural frequency of the wind turbine system. This proximity will also cause the wind turbine system to vibrate constantly. Figure 12 shows the two types of soil–structure interaction: (a) fatigue type (non-inertial and cyclic); (b) and resonance type due to vibration. Fatigue type loading is a large strain and may cause the soil to degrade (i.e., strain accumulation), but the resonance type may cause certain types of soils to heal or recover. It is important to consider both of these mechanisms in scaled model tests. Readers are referred to Chapter 5 of [2] for further details on the interactions.

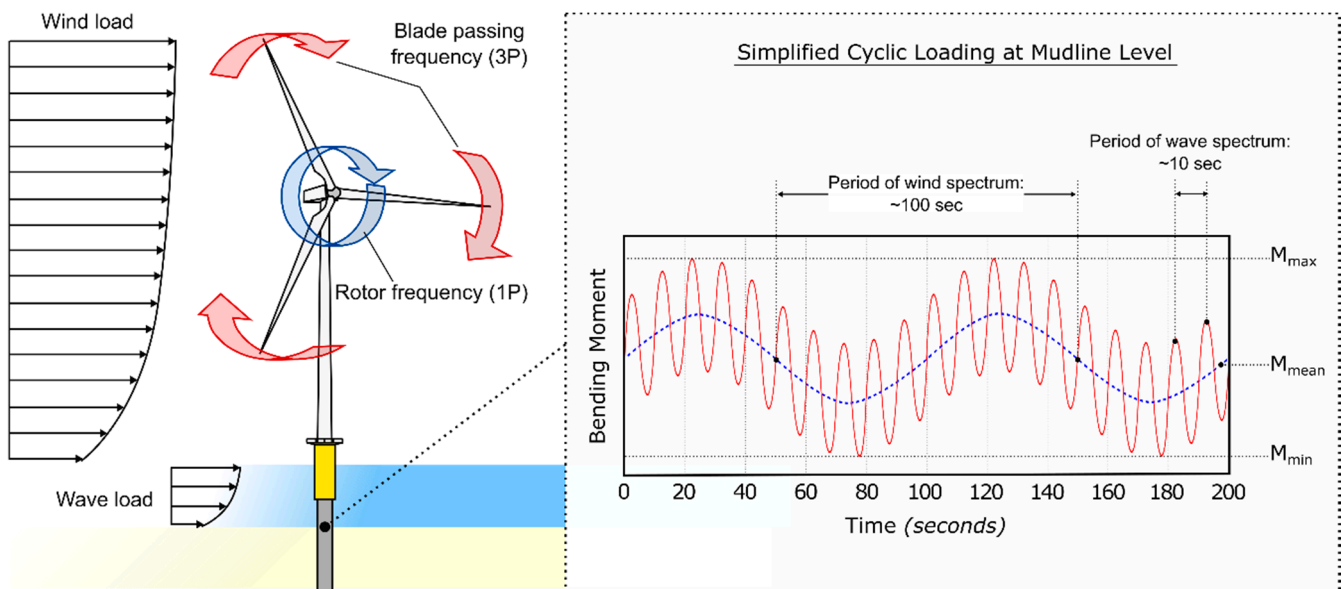


Figure 11. Simplified loading pattern that can be used for scaled model tests.

Behavior of offshore wind turbines involves understanding complex dynamic wind–wave–foundation–structure interaction; the control system onboard the rotor nacelle assembly (RNA) adds further interactions that need to be accounted for. Many new foundations are being proposed for supporting wind turbines in deeper and harsher environments, and this calls for the need for scaled model testing to understand soil–structure interaction. Small scale tests can be used to illustrate the necessary TRL levels listed in Table 1. In particular, physical model testing can be adopted in the following cases:

- (a) Confirmation and validation of the mechanism of load transfer from the superstructure to the ground through the foundation element. This is very important for a new concept of a foundation or a connection. For example, adding a circular plate around a pile may increase the bearing capacity and improve resistance to overturning. Although this is a conjecture, and it must be verified through testing. Furthermore, the long-term effects of the foundation under scour or cyclic loading must be verified.
- (b) Because offshore wind turbines are dynamically sensitive structures, modes of vibration of the structures are very important. These can be carried out through free vibration/perturbation tests or white noise testing. This is an important part of the validation process because modes of vibration can strongly influence the foundation design, fatigue life, and wear and tear of the mechanical components in the RNA.
- (c) Foundations for offshore wind turbines are subjected to hundreds of millions of loading cycles, which can be cyclic or dynamic in nature. Scaled model tests can reveal the expected trends of the behaviour of the foundations due to cyclic and dynamic soil–structure interaction. One of the uncertainties is the long-term non-recoverable tilt of the foundation. Excessive tilt may lead to shut down of the turbine due to loss of warranty.
- (d) The environmental loads transferred to the foundation of offshore wind turbines are very complex; they can be simplified as one-way cyclic or two-cyclic waveforms. The long-term effects of such waveforms can be identified through scaled model tests.
- (e) Due to dynamic sensitivity, offshore wind turbines need damping. Trends and sources of damping can be identified through carefully designed scale model tests.

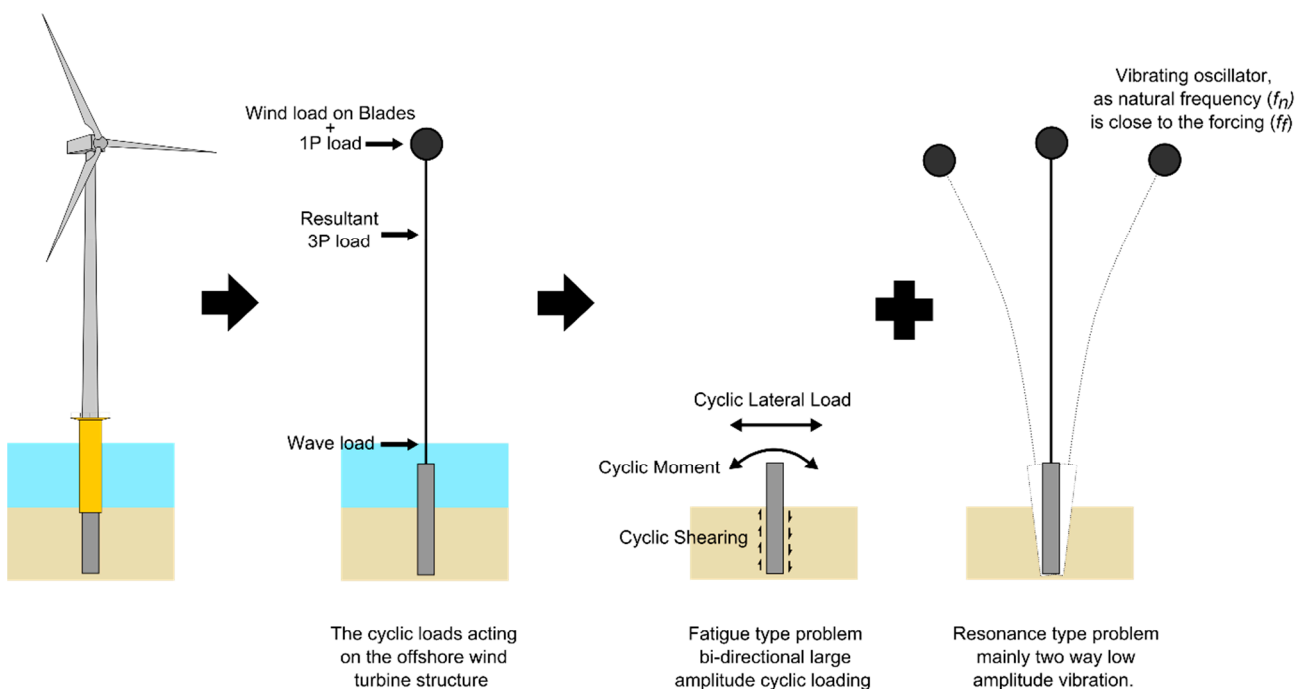


Figure 12. SSI mechanisms.

### 5.1. Types of Scaled Model Apparatus

Based on the literature of physical modelling and in the context of predicting foundation behaviour, the experimental test setup can be classified as follows:

**TYPE 1:** “Foundation only modelling”—referred to as Type 1 as shown schematically in Figure 13a. In this modelling, cyclic loads (e.g., one-way cyclic, two-way cyclic, symmetric, asymmetric, or a combination) can be applied. The limitation of this method is that the effects of vibration of the whole system, i.e., the effects of inertia of the RNA mass, are not modelled. If we were to translate the context and apply the understanding of soil

mechanics, the small strain vibration due to the system dynamics of the wind turbine (i.e., resonance type mechanism in Figure 12) is ignored. For sandy soil, this phenomenon will definitely densify the soil around the foundation. Ignoring such effects will overestimate the tilting prediction (i.e., SLS requirements) of the foundation. However, Type-1 modelling may be appropriate for foundations for floating systems; see Figure 13b, in which the loads on the foundations are applied through mooring lines and dynamic effects can be ignored.

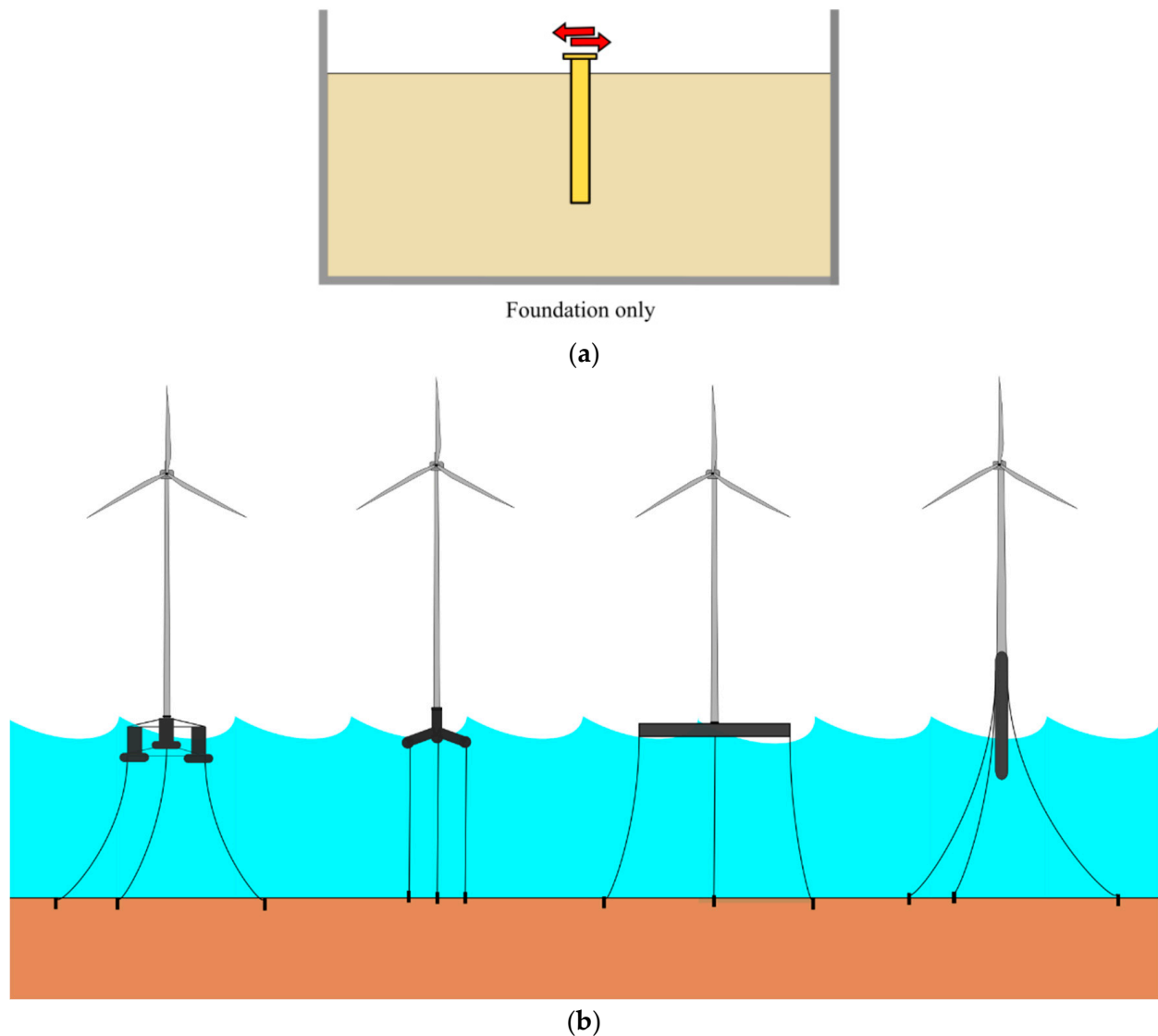


**Figure 13.** (a) “Foundation only modelling”—Type 1 technique. (b) Examples where Type 1 modelling is appropriate.

**TYPE 2:** “Whole system modelling with an actuator (attached with the model with a rigid link)”—referred to as Type 2 as shown in Figure 14a. In this case, the actuator provides lateral stiffness to the overall system, and the effect is distorting the modes of vibration; see Figure 14b,ii for an explanation. Example applications of Type 2 modelling can be found in Lombardi et al. [30], and some examples are provided here in Figure 14c, d. However, this type of modelling is suitable to understand various aspects of damping, i.e., physics of the problem.

**TYPE 3:** “Whole system modelling with eccentric mass actuator”—referred to as Type 3 as shown in Figure 15a–c. Figure 15a shows the schematic representation of the setup. This is currently the most appropriate physical modelling technique, and details can be found in [31]. Type 3 modelling technique is scalable, can model wind–wave

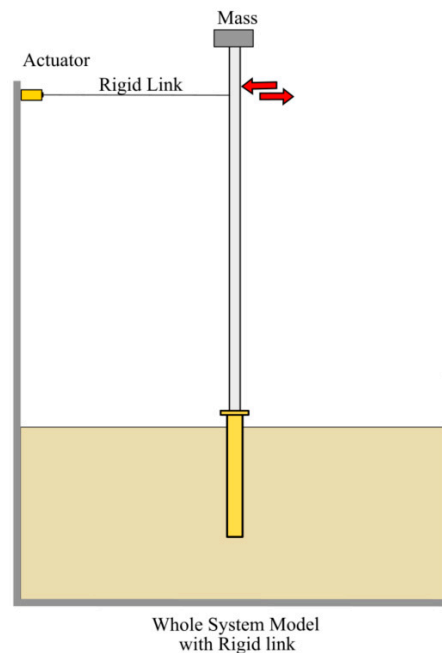
misalignment, can be used in field testing, and can also study fatigue-related issues. Examples of testing using the Type 3 technique can be found in [32,33], and the long-term performance of monopiles was studied by [34], in which the fatigue problem was studied using the apparatus (for further details, see Figures 16 and 17).

### 5.2. Measurement of Dynamic Response and Type 2 Technique

One of the important considerations is the change in dynamic performance due to the application of cyclic loading. This change may be significant in the presence of loose deposits, which may liquefy as a result of cyclic loadings [26,35–37]. One of the ways to quantify this is monitoring the change (if any) of the natural frequency and damping of the system after cycles of loading. Although this can be cumbersome because these tests may need to run for a long time, it is often desirable that the process could be automated, such as by means of white noise testing.

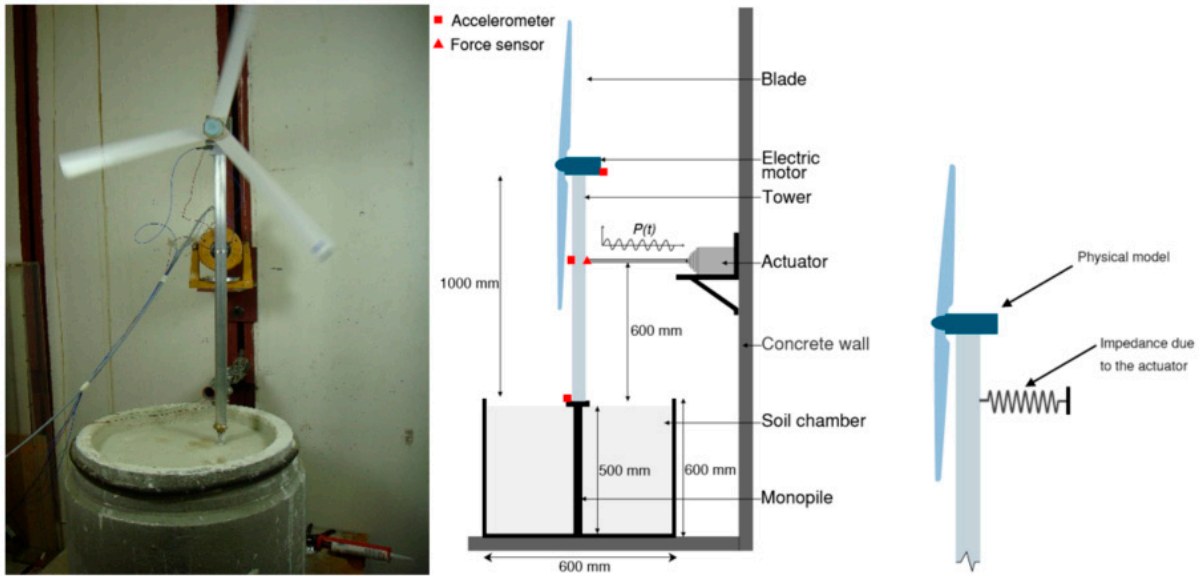
#### White Noise Testing

White noise testing is a method of measuring dynamic properties in the frequency domain by producing a response spectrum. The system in question is excited by a white noise signal (that is, a signal which theoretically contains equal components of every frequency in a certain range) and an accelerometer attached to the structure to record the resulting movements. Because the power spectrum of the input signal is flat (i.e., constant energy over a certain bandwidth), the power spectrum given by the analysis of the accelerometer signal should be a response spectrum of the system whereby its peaks correspond to the resonant frequencies. In reality, the input signal can only be an approximation to perfect white noise, and its power spectrum will show some variation of spectral density with frequency. Dividing the output spectrum by the input spectrum can compensate for this. For a white noise test, the damping must be calculated in the frequency domain. This is undertaken by measuring the width of the frequency peak on the power spectrum of the signal, and the measurement can be used to evaluate the ratio of critical damping.

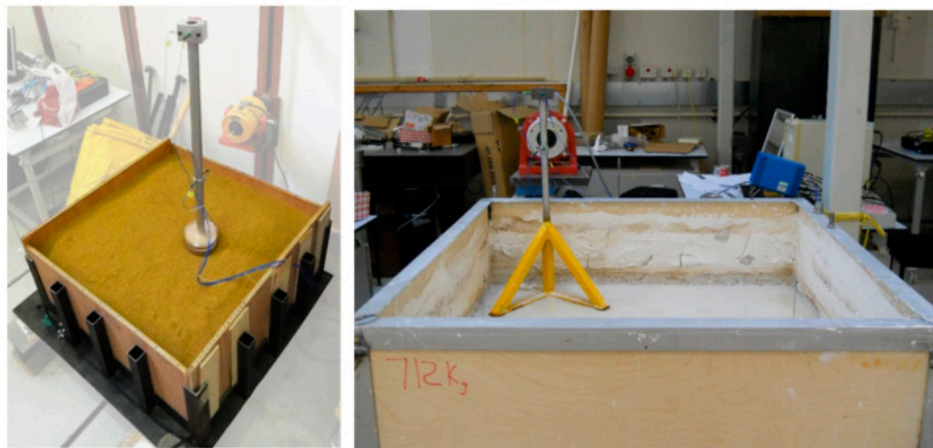


(a)

Figure 14. Cont.

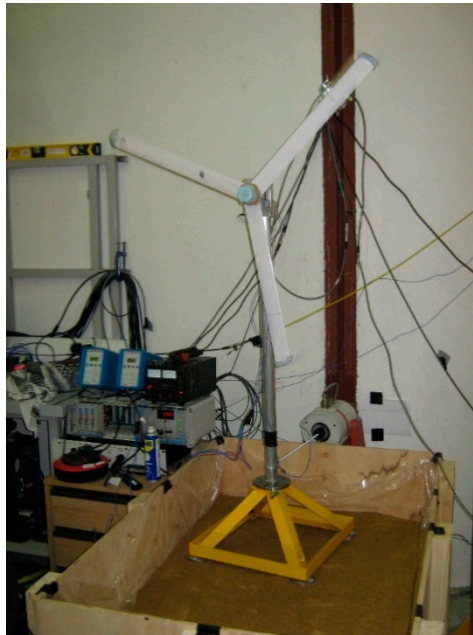


(b)



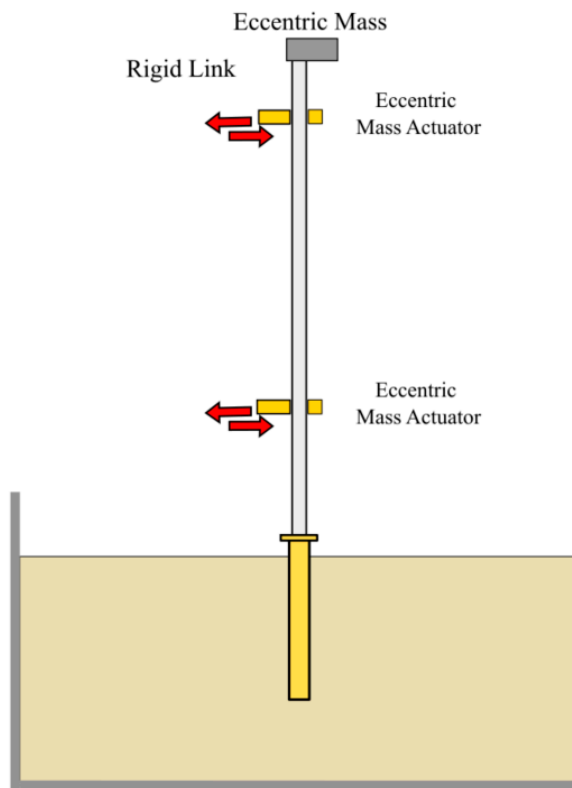
(c)

Figure 14. Cont.



(d)

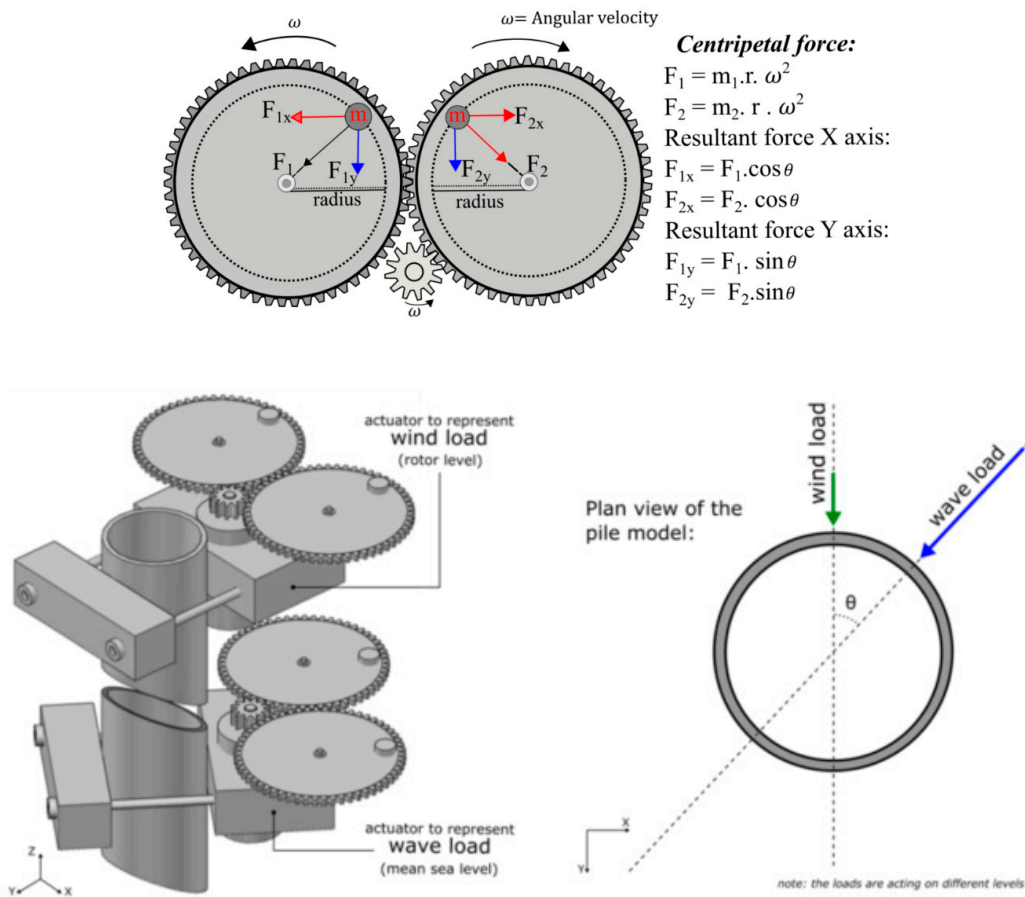
**Figure 14.** (a) “Whole system model with an actuator connected to the model through a rigid link”—Type 2 technique. (b) Model setup and instrumentation used for small-scale wind turbine supported on a monopile: (i) photograph and schematic diagram; (ii) Impedance in a rigidly connected actuator [30]. (c) Other applications for Type 2 modelling. (d) Example application of the Type 2 technique.



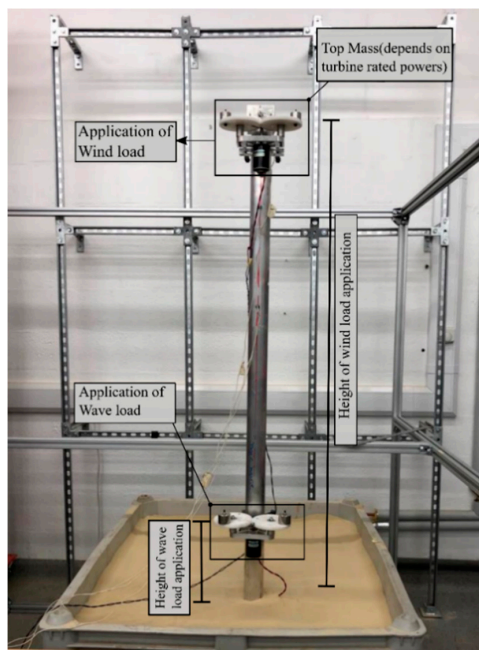
Whole System Model with eccentric mass actuator

(a)

**Figure 15.** *Cont.*



(b)



(c)

**Figure 15.** (a) Whole system modelling with an eccentric mass actuator (Type 3 technique). (b) Working principle of the loading device. (c) Example application of the Type 3 Technique.



Figure 16. Examples of the Type 3 technique used in Zhejiang University (China).

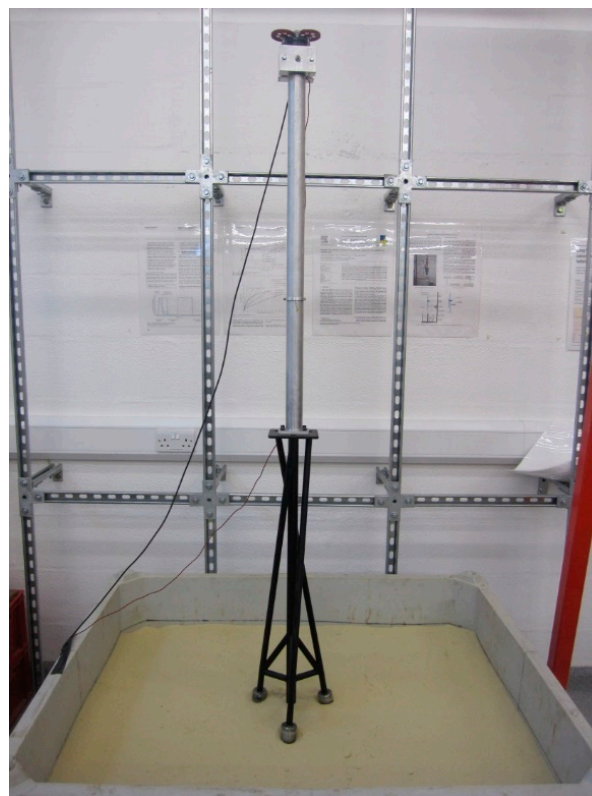
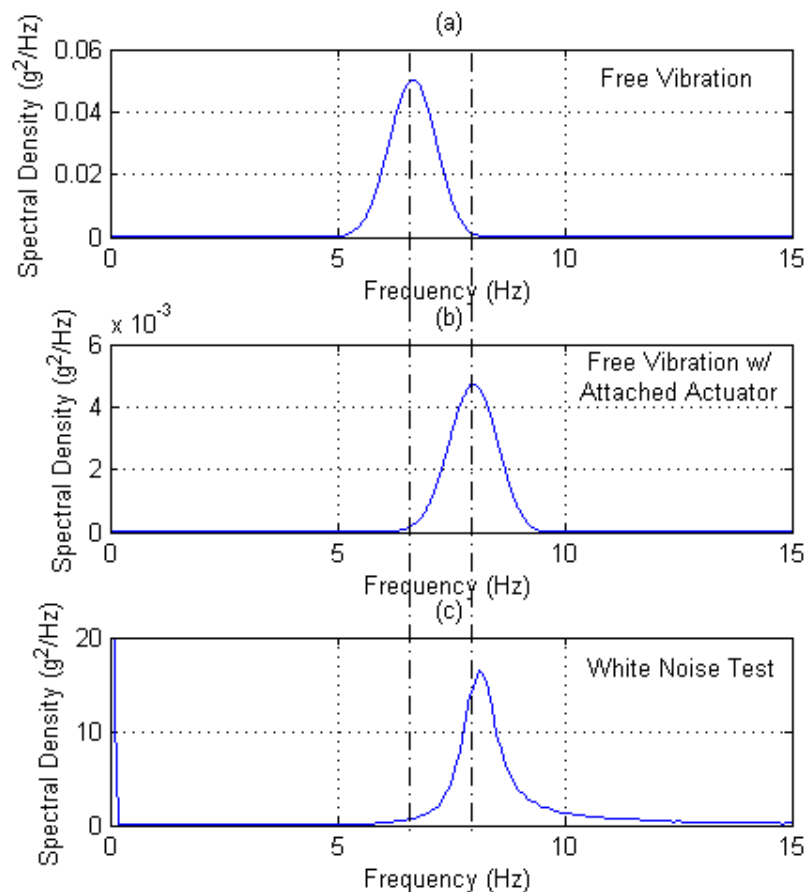


Figure 17. Jacket on slender piles (Surrey Advanced Geotechnical Engineering Laboratory) using Type 3 modelling.



White noise testing was trialed because it offered the possibility of acquiring data at more frequent intervals during long-term tests due to its greater potential for automation over free vibration tests. It also allows narrower frequency bands in the frequency-domain plots, allowing better estimation of the natural frequency of the system because white noise testing may be continued for as long an interval as desired, whereas free vibration tests can last only as long as the vibrations induced in the apparatus. A system can be developed in which the cyclic loading is interrupted at regular intervals by white noise tests, the results of which can be automatically recorded and analyzed (Figure 18).



**Figure 18.** Comparison of dynamic responses (using signal filtering to remove non-tower modes) of a monopile foundation gained using: (a) standard free vibration method, (b) free vibration method with attached actuator rod, and (c) white noise method.

Our extensive experience with small-scale tests showed that connecting the actuator rod to the tower modified the natural frequency of the system significantly (in one case from 6.5 to 8 Hz) as a result of the added stiffness of the actuator; damping was also increased. This effect was found to be greater if the actuator connection was moved up the tower, as dictated by fundamental dynamics, because the mode shape displacement increases with the increasing height of the tower. This implies that the evaluation of natural frequency and damping of the free system during an experiment requires significant post-processing of results and is undesirable. The Type 3 technique removes all of the above effects.

### 5.3. One the Use of “Reductionist” Approach [Type 1 versus Type 3] for Grounded System

The Type 1 apparatus is an example of “reductionist” approach, which means the whole offshore wind turbine system is tested by individual components whose findings are related to one another to determine the overall response of the system. In the context of an offshore wind turbine, an individual component may comprise the foundation and the supporting soil (as per the Type 1 problem). This approach may fail for problems related

to offshore wind turbines (or any structure subjected to multiple interactions) because it may not be possible to separate out the individual components due to the interaction between complex loading histories and non-linear material, in addition to geometries. The reductionist approach works well for linear problems, i.e., where superposition principles apply. Designing scaled model tests involving many interactions is therefore challenging.

### 6. Example of Scaled Model Tests

This section of the paper presents examples on the use of scaled model tests and the purpose of the tests.

#### 6.1. Proof of Concept of Floating Systems

Figure 19a shows a schematic of a scaled model of a floating system. The main aim of this study was to understand the stability of the system and identify the features that enhance stability. In this problem, different arrangements of anchoring were tested, and the effectiveness of the bottom weight was also verified. This can constitute the initial part of TRL, i.e., basic principles are verified in terms of equilibrium and stability. Figure 19b shows the acceleration response, and many such tests can be carried out to understand the limits of stability.

#### 6.2. Example of Scaled Test on Biofouling on Monopiles

Figure 20 shows another example of TRL testing on measures to mitigate biofouling on monopiles carried out in Ireland.

#### 6.3. TLP Experiment

This is another example of a TRL level study for the TLP-type of platform; further details can be found in [38] (see Figure 21).

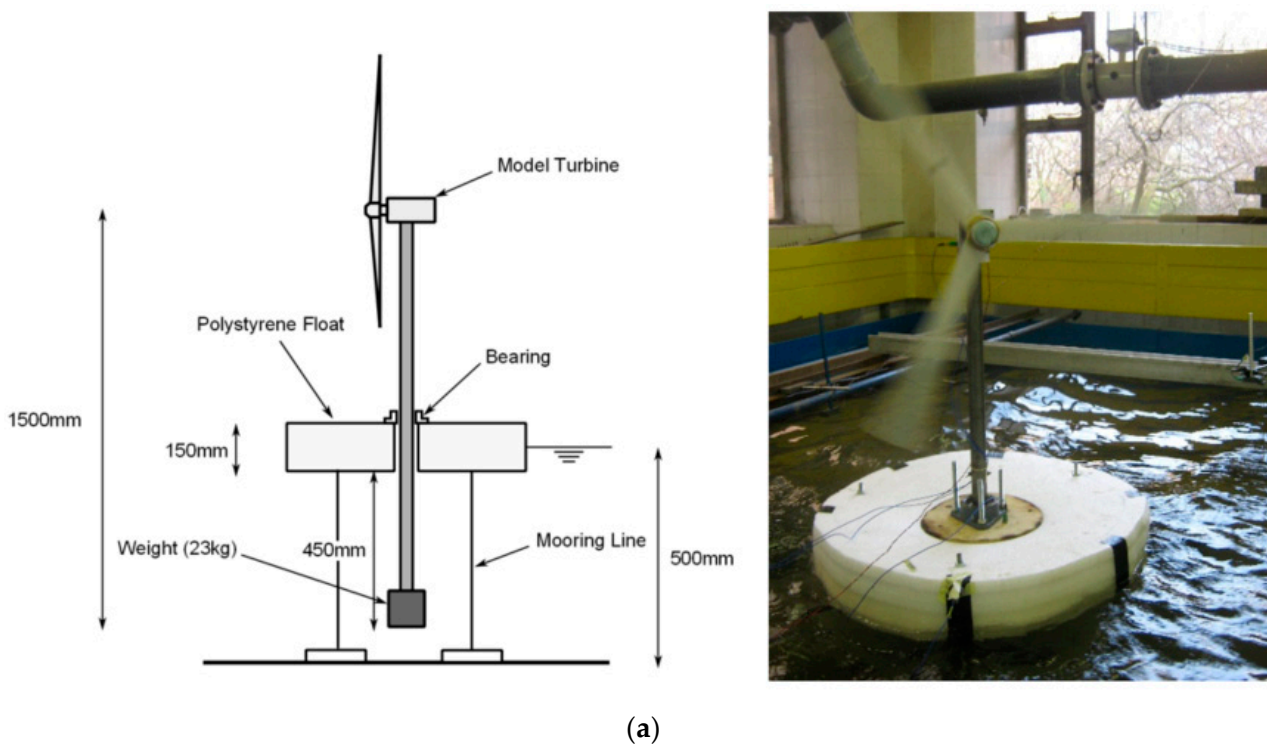
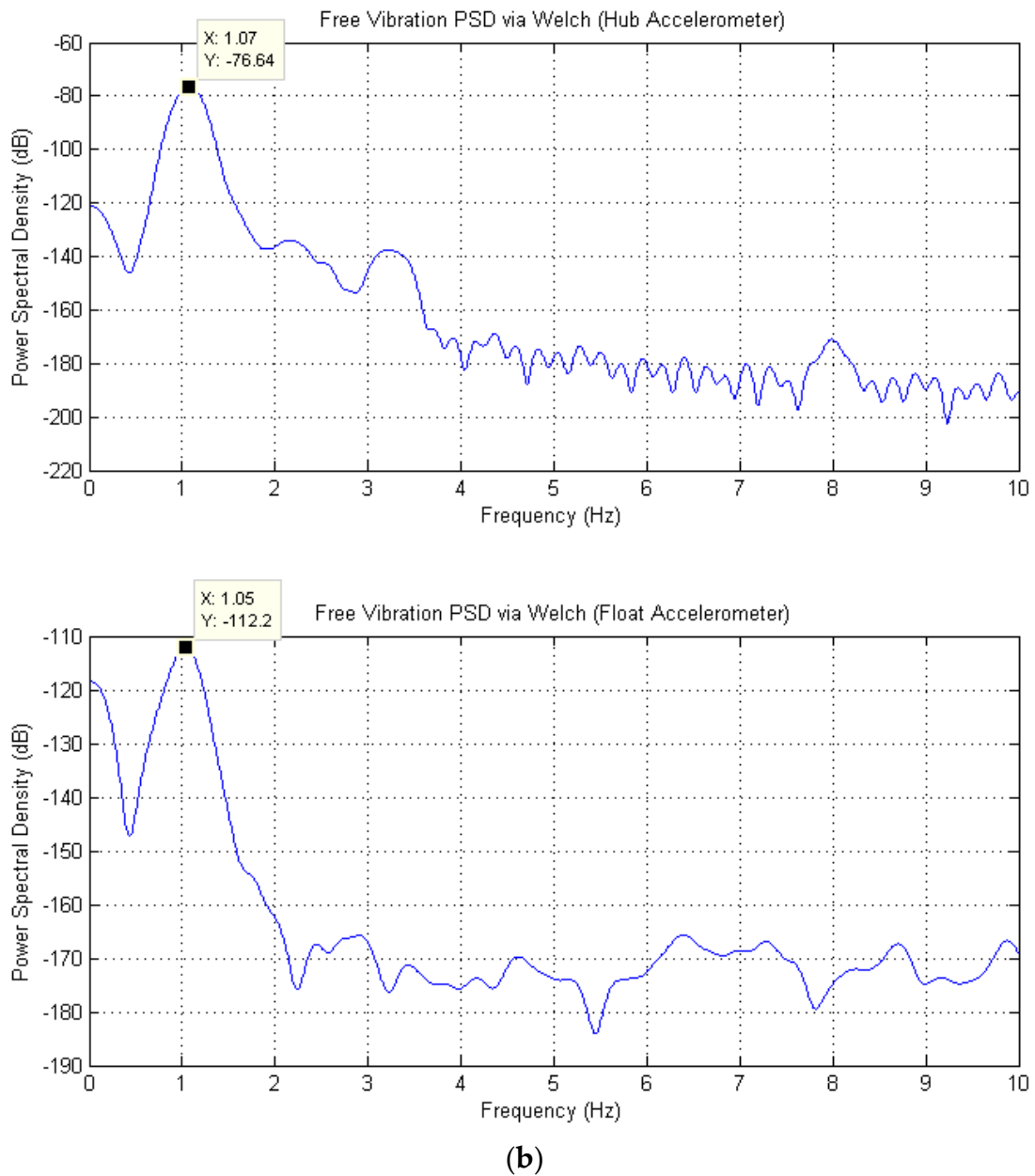


Figure 19. Cont.



**Figure 19.** (a) Proof of concept of floating wind turbine systems. (b) Measurements from the accelerator of the hub and the float.

#### 6.4. Verification of Failure Modes of Anchor Foundations for Spar Type

One example of the usefulness of physical modelling is taken here in relation to a spar-type floating wind turbine. Physical modelling was conducted to understand the optimum location of the padeye, i.e., where the chain will be attached to the anchor piles and what failure mechanism may be invoked; see Figure 22a. A second purpose was to examine the deformation mechanism of soil around the foundation. Figure 22c notes the observed modes of failure. Knowledge from this understanding was used (without scaling any numbers) to develop a design method, as found in [39]. The method was calibrated and compared with the Hywind Wind Farm project.

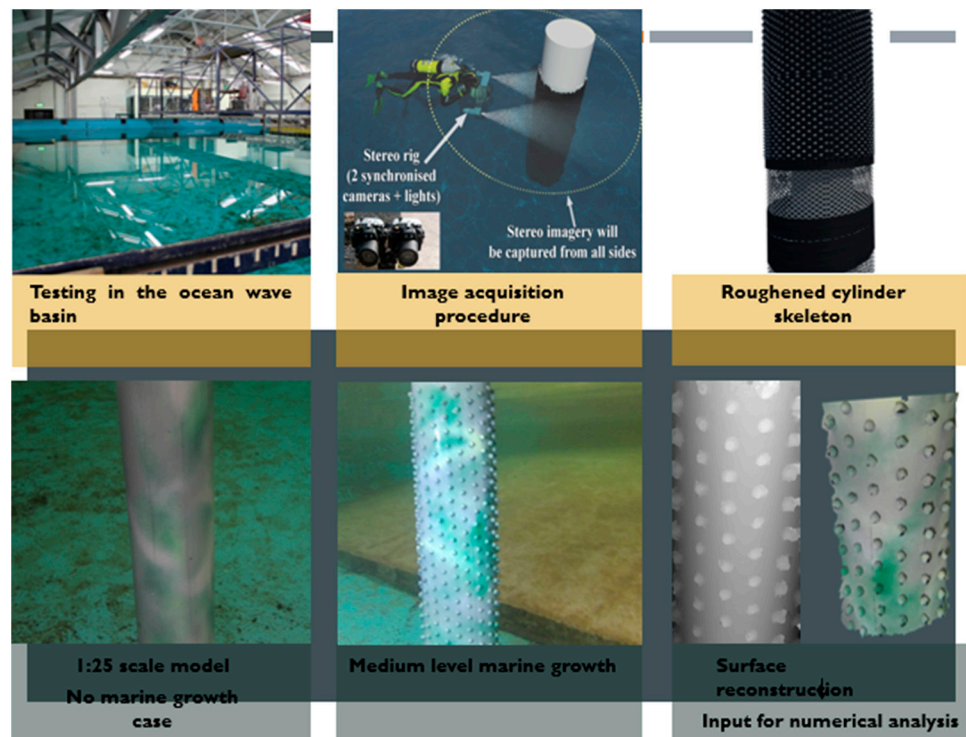


Figure 20. TRL testing for biofouling.

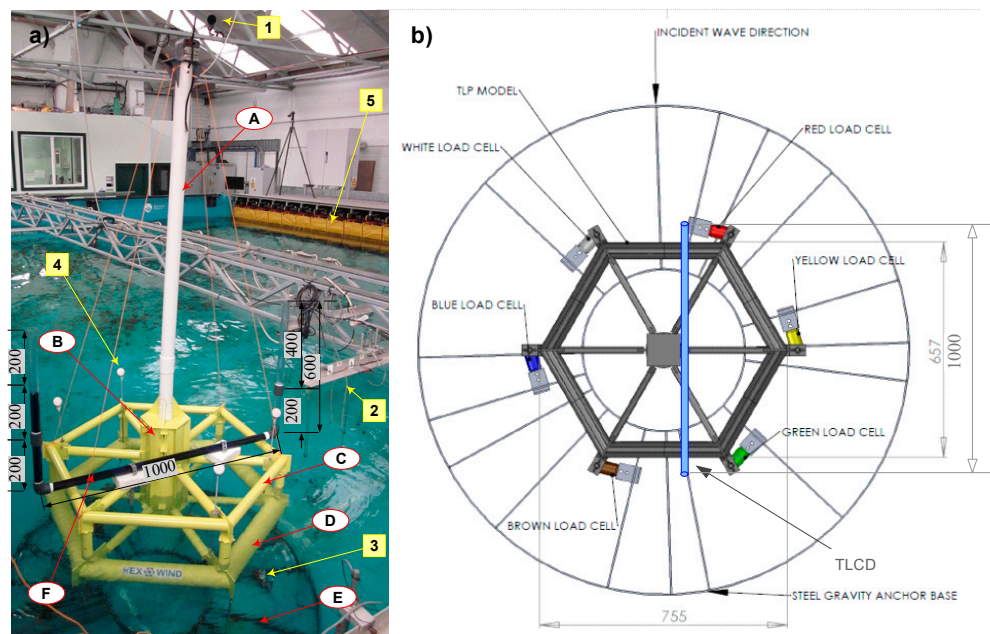
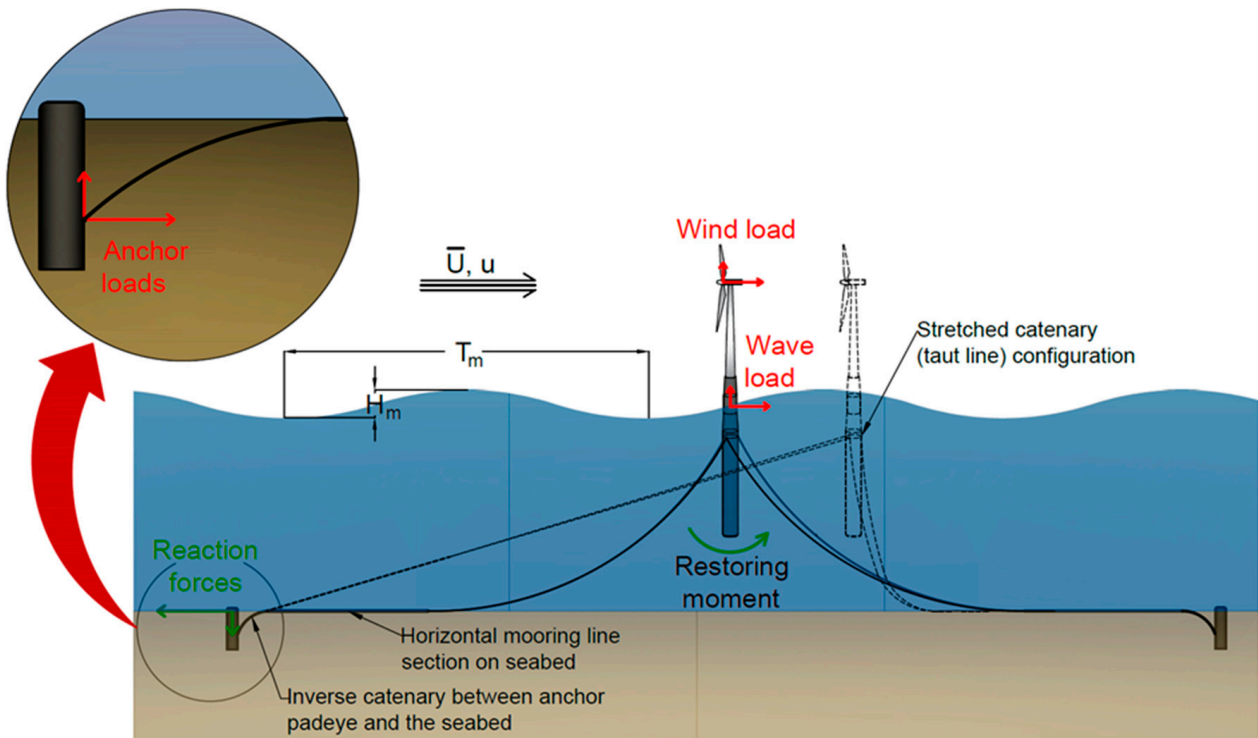


Figure 21. Example of TLP testing. (a) 1:50 scale model of truss-type TLP platform experimental setup: (A) mast, (B) central column, (C) upper structure, (D) buoyancy ring, (E) gravity base, and (F) TLCD. The locations of devices used: (1) motion camera, (2) wave probes, (3) load cells, (4) reflective motion markers, and (5) flap-type wave-maker; (b) TLP view from above: position of TLCD and gravity base with load cell arrangement in relation to the incident wave direction (reproduced from [38]).

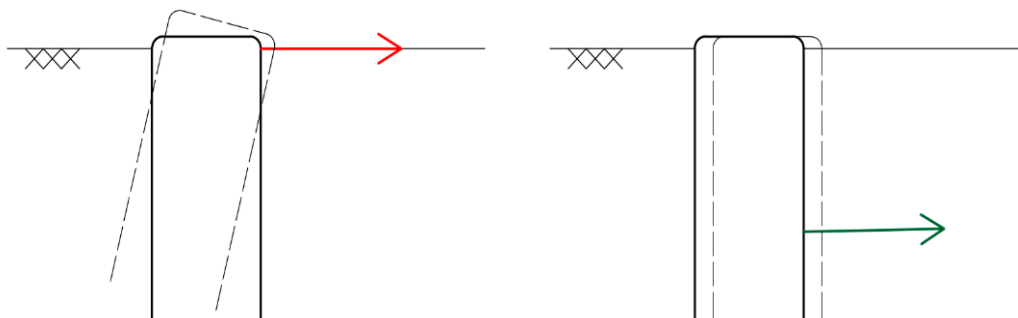
### 6.5. Modes of Vibration of Systems

Modes of vibration are important in design because they affects FLS and, to some extent, SLS. Free vibration testing is used to understand the modes of vibration. In this method, a small displacement/perturbation is applied to the tower manually, and the tower is then released and allowed to vibrate freely—this is often known as the snap-back test. An accelerometer is used to measure the movement this induces, which will occur at the resonant frequencies of the system because no force is involved. Analysis of the signal will provide the damping and resonant frequencies of the system and can be performed in either the time domain (through measurement of peak-to-peak distances) or the frequency domain (by finding a power spectrum). The power spectrum of each signal was obtained through a fast Fourier transform using the method proposed by [40]. Free vibration can be carried out on a range of scaled model tests to understand the modes of vibration and how they evolve with cycles of loading. There is an important scaling law that must be maintained in order to recreate the modes of vibration.



I. Rigid body rotation

II. Horizontal translation



(a)

Figure 22. Cont.

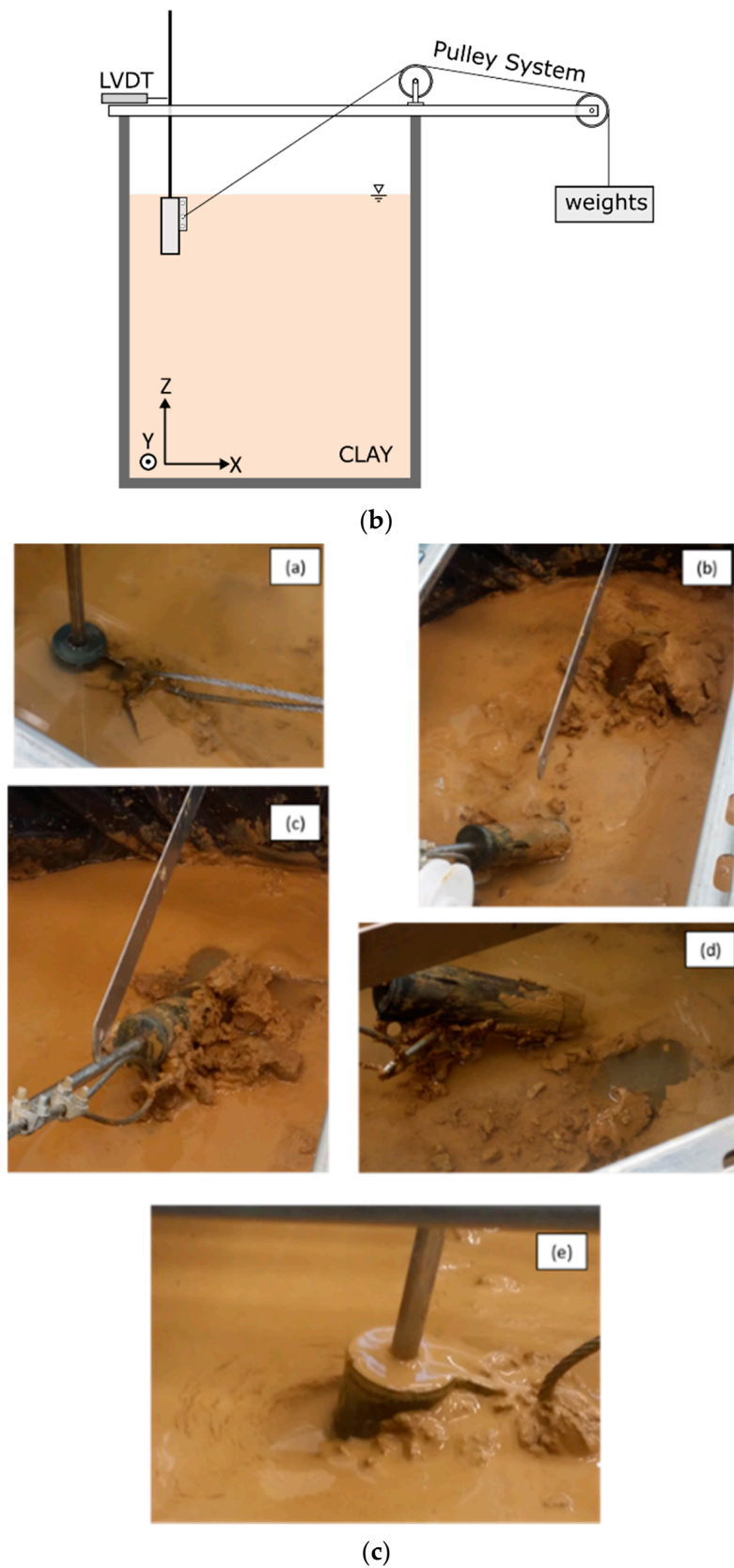


**Figure 22.** (a) Load transfer to the anchor and to verify the above hypothesis of failure mechanism. (b) Schematic of the test setup. (c) Example of understanding the failure mechanism of the anchor for different locations of the padeye.

Scaling laws for modelling modes of vibration: to capture the modes of vibration, one needs to have the following similarities:

- (a) Mass similarities, i.e., mass distribution along the length of the tower;
- (b) Stiffness similarity, i.e., relative tower to foundation similarity;
- (c) Geometric similarity, i.e., the relative distance between the foundation in proportion to the tower must be preserved.

Readers are referred to [41] for further details. Damping is an important consideration for design and plays an important role in FLS and SLS calculations. This calls for benchmark tests, and one of the proposed approaches is to carry out the fixed base frequency of the system and compare it with overall observed behaviour considering the SSI. Figure 23b shows a model by which the fixed base frequency is obtained for the monopile system before the foundation is embedded in the sand chamber.

There are two main types of vibrations that affect the design of offshore wind turbines:

- (a) Sway-bending, i.e., flexible modes of the tower without rocking modes of foundations. This is typical of any wind turbine systems on deep foundations. Figure 23c shows an example of a twisted jacket on pile foundations where the first mode is distinct from the second mode.
- (b) Rocking mode of vibration, which occurs due to the rigid rocking of foundations and will be manifested with two closely spaced modes. Figure 23d,e shows two examples. For the symmetric arrangement of foundations (i.e., tetrapod), the initially observed closely spaced peaks will merge into a single peak after tens of thousands of cycles. However, for asymmetric systems (i.e., the system shown in Figure 23e), these peaks converge.

Readers are referred to Chapter 3 of Bhattacharya [2] for a comprehensive review of the modes of vibration. It must be mentioned that the rocking modes of vibration are usually low-frequency modes and can be tuned with the 1P rotor modes aggravating the FLS issues. One of the important aspects of TRL studies is to verify and validate the modes of vibration obtained from the numerical work.

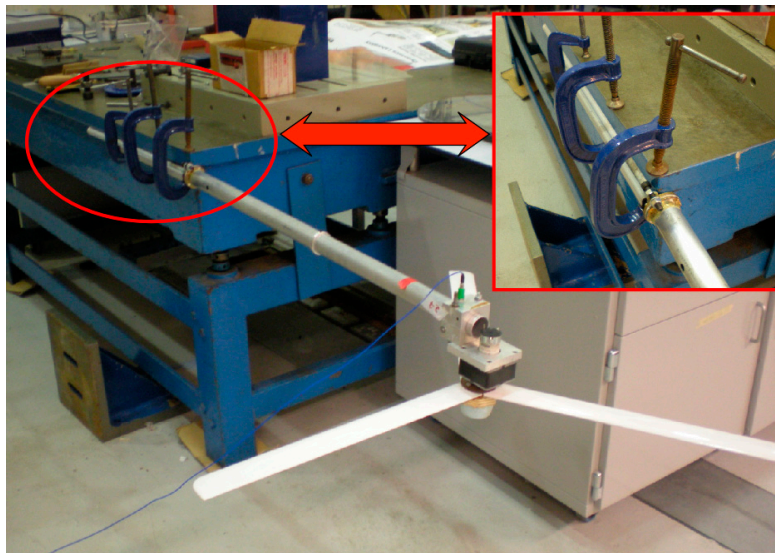
Figure 24 shows an example of the long-term performance of a wind turbine system (wind turbine model in a tetrapod where the foundations are suction buckets) whereby the change in natural frequency is noted for millions of cycles of loading. As expected, the modes of vibration were rocking modes, and the tests were conducted on loose soil, dense soil, dry soil, and saturated sand matrix. The purpose of the tests was to understand the different aspects of (cyclic and dynamic) soil–structure interaction (SSI) behavior rather than replicating a particular field problem. The scaling of understanding gained to predict the prototype behaviour is beyond the scope of the current paper.

### 6.6. Centrifuge Modelling

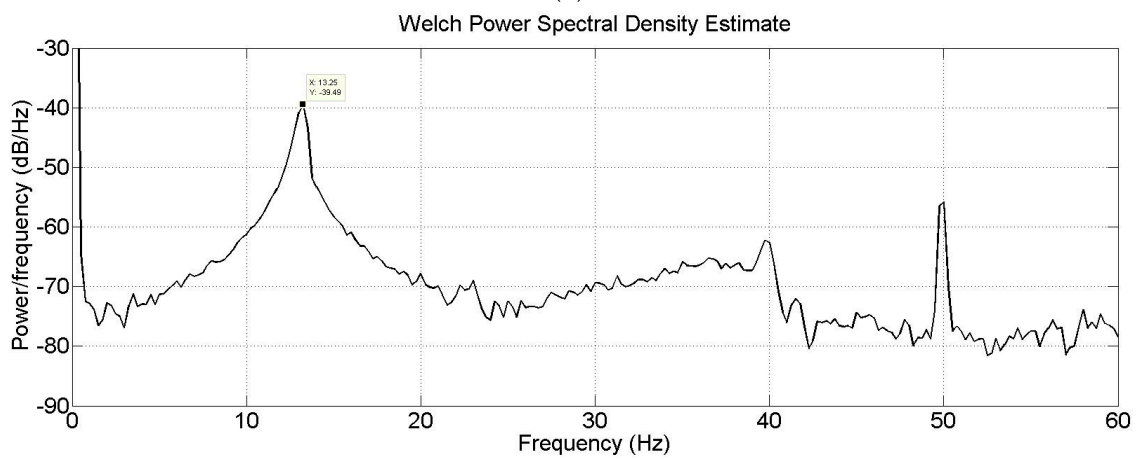
Centrifuge geotechnical modelling is an established physical modelling technique to test materials whose mechanical properties are stress dependent. In particular, to replicate the geostatic stress conditions existing in the field in a small-scale experiment, the model is rotated at a certain angular velocity  $\omega$  that results in an acceleration field  $N$  times that induced by the gravitation acceleration  $g$ . A view of the model container tested in the geotechnical centrifuge at the University of Manchester is shown in Figure 24. To apply cyclic actions representing the environmental loads induced by wind and waves, the model can be loaded with an electrodynamic actuator such as the one shown in Figures 25 and 26. Readers are referred to the centrifuge work of Cox [42] for centrifuge modelling work on a shallow foundation.



(a)



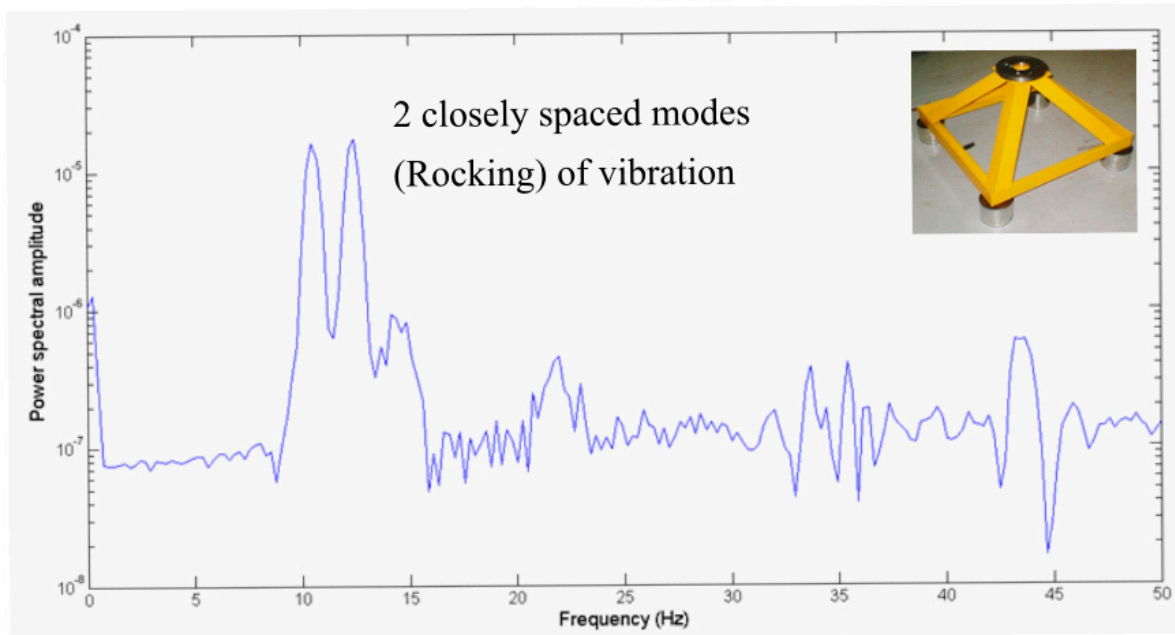
(b)



(c)

Figure 23. Cont.



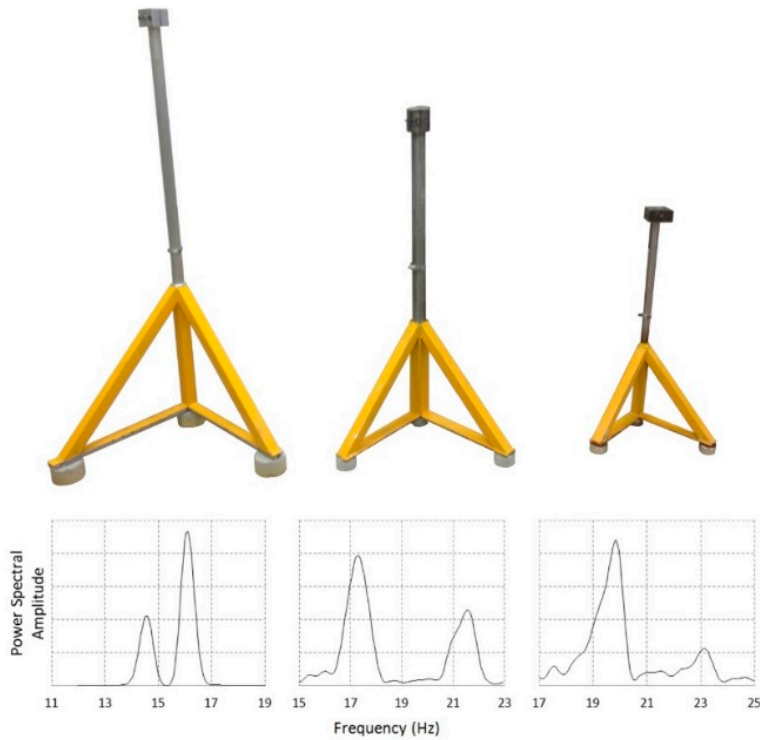


(d)

Scale 1:100

1:150

1:200



(e)

**Figure 23.** (a) The shallow foundation models studied. (b) Free vibration test to obtain fixed-base frequency. The test helps to identify the role of foundation plays in overall damping. (c). Welch power spectral density estimate obtained through the free vibration test of the twisted jacket foundation after 25,000 loading cycles (See Figure 14 for the model). (d) Free vibration response of the tetrapod structure in Figure 17 (e) Modes of vibration with two closely spaced modes.

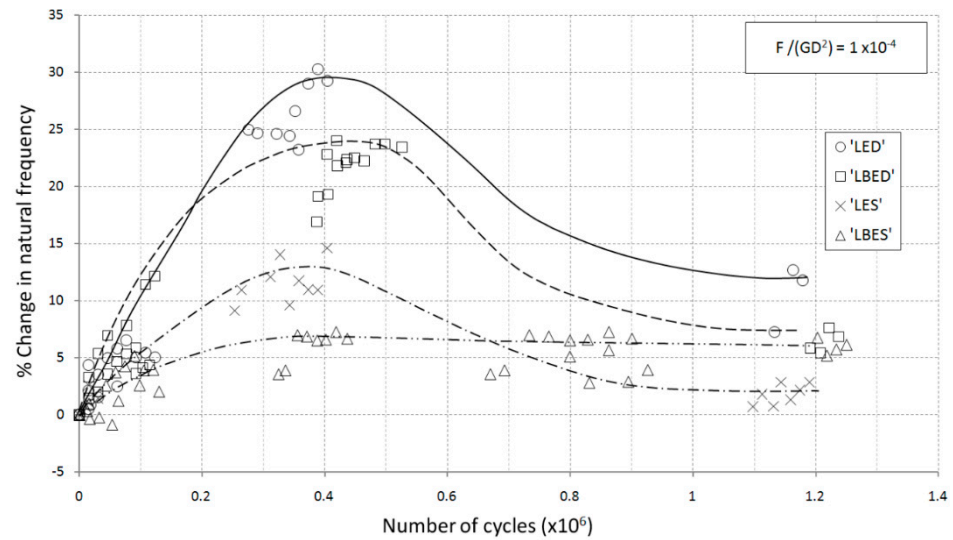


**Figure 24.** Long-term change in natural frequency of a tetrapod foundation (Figures 9 and 14d) for different ground profiles indicated by LED, LBED, LES, and LBES.

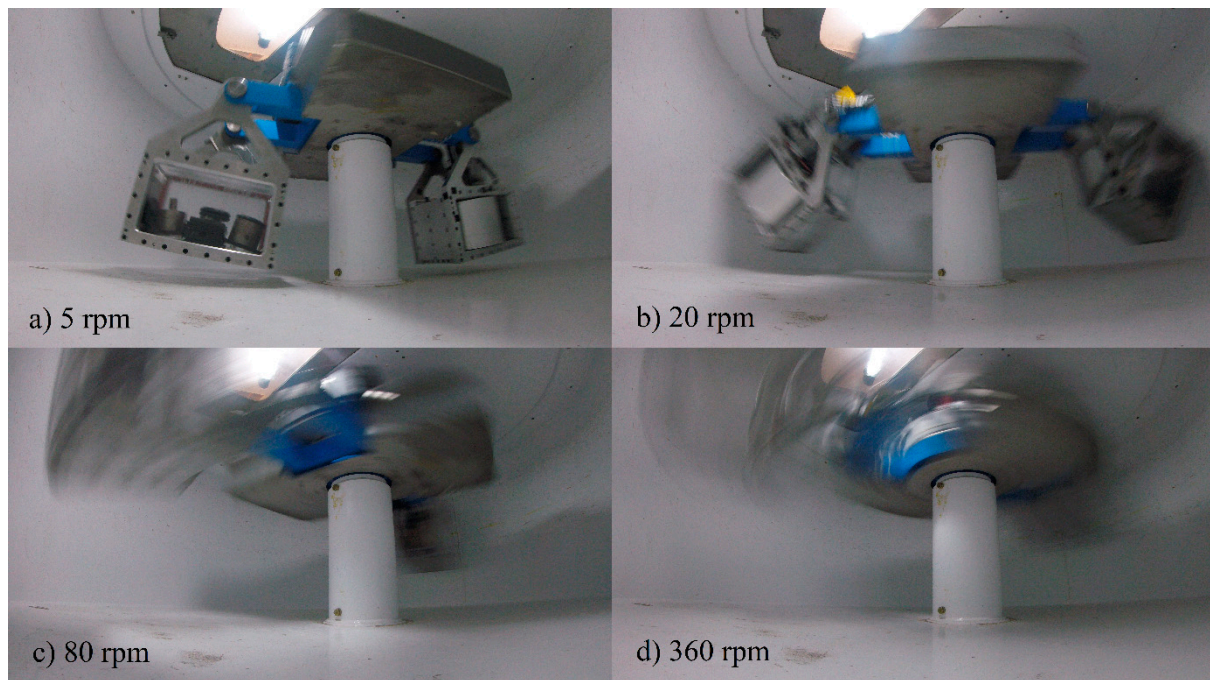


**Figure 25.** Model container installed on the beam centrifuge at the University of Manchester: (a) 5 rotations-per-minute; (b) 20 rotations-per-minute; (c) 80 rotations-per-minute; (d) 360 rotations-per-minute.

### 6.7. Earthquake Response of Wind Turbine Structures

Regardless of whether the tests are carried out using shaking tables at normal gravity or geotechnical centrifuges, the soil deposit needs to be confined in a container with relatively small dimensions. A significant challenge encountered when performing geotechnical physical modelling is to simulate free-field seismic conditions and reduce the boundary effects introduced by the rigid wall of the model container. The vast majority of research activities in earthquake engineering are based on the simulation of an idealized infinite lateral extent soil stratum that overlays the bedrock, which is shaken at its base (see Figure 27). Over the past decade, researchers have developed different types of model container to minimize the effects introduced by the artificial boundaries. The reader is

referred to [43,44] for a detailed review of the possible boundary solutions available for physical modelling testing.

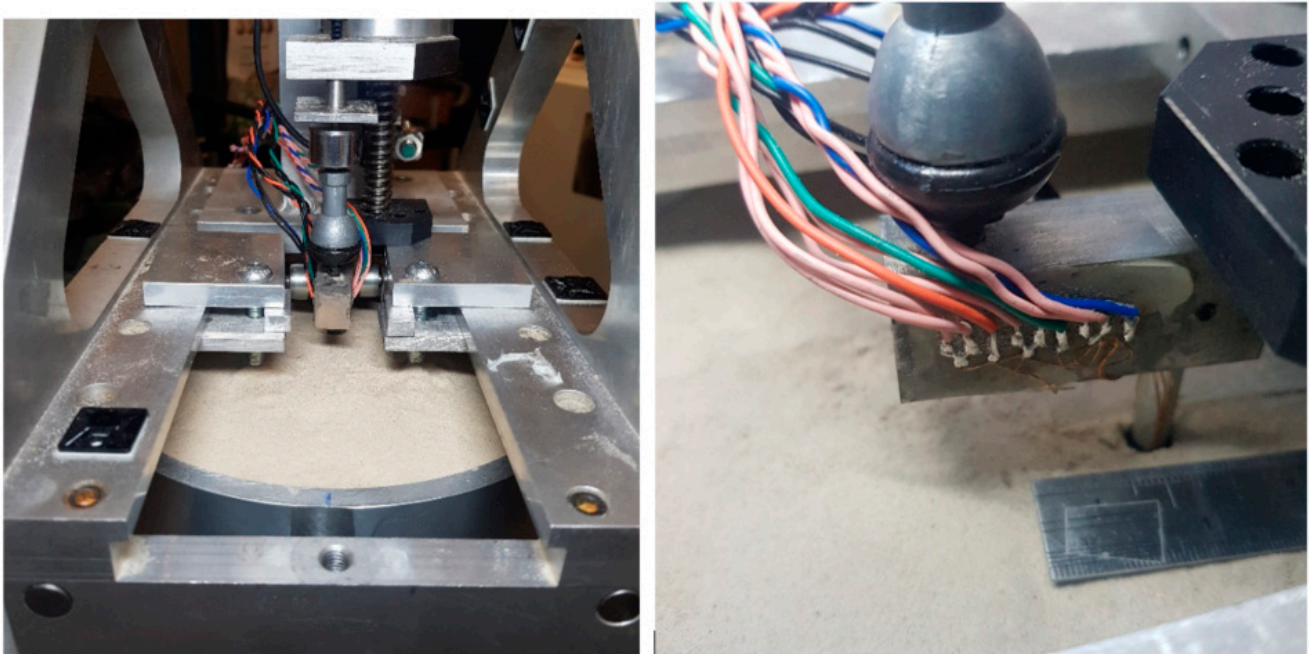


Figure 26. Example of experimental setup used in testing laterally loaded piles in the geotechnical centrifuge of the University of Manchester.

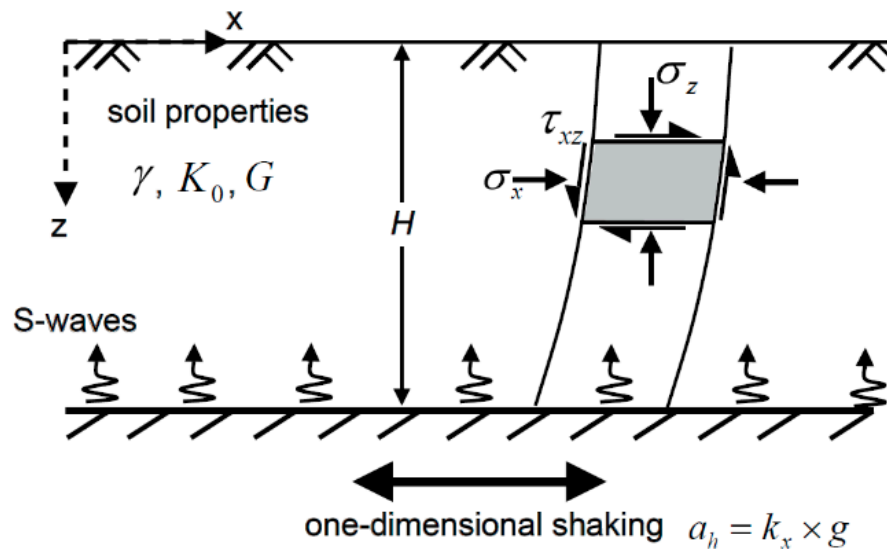
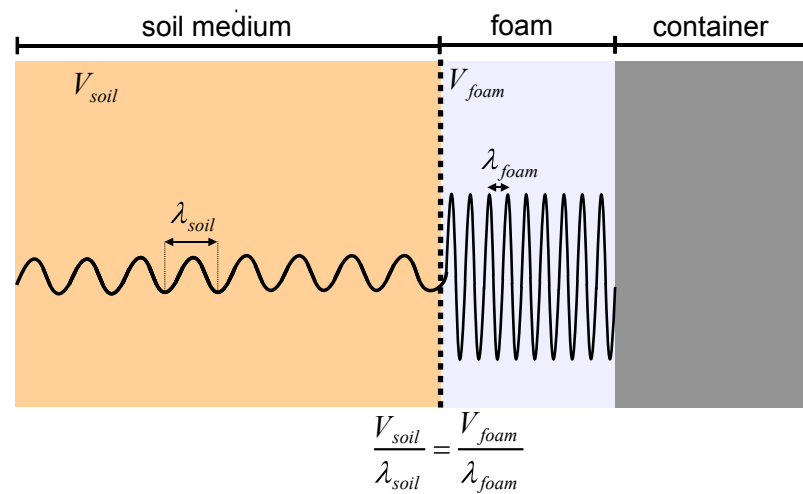


Figure 27. Shear-beam idealisation of infinite lateral extent stratum overlying a bedrock subjected to one-dimensional shaking.

There are critical aspects when choosing the model container for dynamic tests. Some dynamic tests are subjected to one-dimensional motion; when a body wave encounters the interface between media having different impedances (i.e., soil–wall interface), the wave energy is partially reflected and partially transmitted through the boundary. Wave mode conversion therefore occurs, whereby P-waves are converted into S-waves and vice-versa. However, in the case of a rigid box with absorbing boundaries (see Figure 28), as the P-wave propagates from the soil into the foam layer, the velocity of propagation slows down due to the low impedance of the softer material [45]. At the interface, the frequency of the propagating wave ( $f = V/\lambda$ , where  $\lambda$  is the wavelength) must remain constant. Therefore,

when the wave propagates from the soil medium into the foam, the wavelength must decrease. This reduction in wavelength can be associated with energy dissipation [45].



**Figure 28.** Schematic of wave propagation within a soil container having absorbing boundaries.

The analysis of strong ground motion data, whether from physical measurements or numerical modelling, most likely exhibits the following issues: (i) limited time span of data with meaningful information, i.e., short records with high signal-to-noise ratios; (ii) intrinsic non-stationary of the data; and (iii) intrinsic nonlinearity of the process being recorded. The Fourier spectral analysis has been widely used for computing the energy-frequency distribution of strong ground motion data, although the method is strictly applicable to linear systems and time-series characterized by ergodicity and stationarity. In earthquake engineering, the conditions of linearity and ergodicity are rarely met because most of the available data is transient in nature and intrinsically non-linear. The requirement of stationarity may be satisfied by assuming that data is stationary within a limited time span (i.e., piecewise stationarity) or data becomes stationary when the time approaches infinity (i.e., asymptotically stationarity). When the Fourier spectral analysis is applied to data that do not satisfy these assumptions, the Fourier transform introduces spurious harmonic components that artificially widen the frequency spectrum.

A number of data processing methods for non-linear and non-stationary processes are available, including (i) the Wigner–Ville distribution method, which is widely used by the electrical engineering community [46]; (ii) empirical orthogonal function expansion, a method popular in remote sensing, with applications in oceanography and meteorology research [47]; (iii) the Hilbert Huang method [48], which has been applied to a number of geophysical datasets and used for atmospheric and climate studies [49]; and (iv) wavelet transform [50], whose applications to earthquake, wind, and ocean engineering research can be found in [51]. Of particular relevance to the current study is the application of wavelet transform to the analysis of the energy-frequency distribution of earthquake records [52] and spectral non-stationary due to propagation of seismic waves through soft deposits [53]. In contrast to environmental loads, earthquake input motions have multiple frequencies, typically ranging from 0.5 to 10 Hz. Considering the typical wind turbine presented in Table 1, system dynamics scaling laws can reveal that the ratio of forcing frequency (i.e., earthquake frequency), and the natural frequency of the turbine is in the range of 1–16. The typical frequency of the blades is about 1 Hz, which is well within the earthquake frequency.

The authors have extensive experience in testing small-scale model wind turbines on a shake table (see Figure 29). Before the shaking is applied, it is important that the natural frequency of the system is measured using the snap-back test, in which the frequency can be obtained from a free-decay response using either frequency- or time-domain methods (for more details, the reader is referred to [54]). During the shaking, the natural frequency

of the system can be calculated using transfer functions in the frequency domain (see Figure 30).



Figure 29. Illustration of the model wind turbine positioned on the BLADE shaking table.

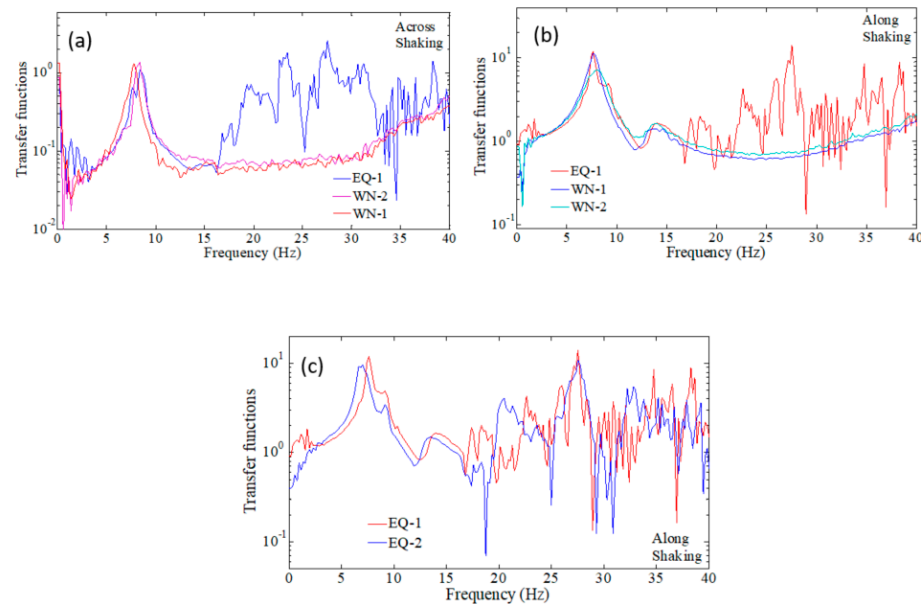


Figure 30. Transfer function estimates for the (a) across shaking direction during the loading states EQ-1, WN-1, WN-2; (b) along shaking direction during EQ-1, WN-1, WN-2; (c) along shaking direction during EQ-1, EQ-2.

From the results are shown in Figure 30, it can be seen that for the across shaking direction, the natural frequency increased from 7.7 Hz in the first test WN-1 to 8.4 Hz in the final test WN-2. Such a change can correspond to a densification of the soil, which stiffens the global wind turbine response. Interestingly, during the actual shaking (EQ-1), two peaks emerged in the relevant transfer function estimates. The first (7.62 Hz) is at a frequency lower than even the initial state estimate at 7.7 Hz, whereas the second is roughly near the final measured state. A very similar picture also holds true for the perpendicular along the shaking direction, as seen in Figure 30b. Intriguingly, one possible explanation for this phenomenon is that it is an amplitude dependence sign, where increasing levels

of stress lower the responding frequencies. Alternatively, it may be a case in which the soil–structure interaction during shaking is correlated with the motion, thus contributing effective stiffness that can additionally alter the dynamic performance. Figure 30c shows some hints of the effect of amplitude on response. For the larger amplitude shaking, EQ-2, the lowest attained frequency shifted even lower to 6.8 Hz, whereas the higher second response peak remained virtually unchanged.

The dynamics of wind turbines appear to face a number of unresolved issues. Previous research work aiming to accurately account for resonance predictions has proved the existence of specific patterns in the change in frequency [43,55]. Here the influence of an earthquake-type loading with a range of loading frequencies under near-resonant conditions showed a multitude of interesting phenomena. Existence of double response peaks, a global stiffening of the response, and, most importantly, the implication of motion-induced forces appear to raise a number of new questions that require further research to answer.

The variation in natural frequency and damping of offshore wind turbines is a crucial issue when the foundation soil liquefies as a result of the accumulation of excess pore pressure induced by the shaking. The authors have carried out numerous tests on both monopile- and pile-supported structures (see Figure 31) and have concluded that the change in natural frequencies is dependent on the excess pore water pressures developed in the soil. Specifically, the natural frequencies reduce considerably with the onset of liquefaction and, at full liquefaction, the frequency may reduce to more than half of the initial value measured before liquefaction. The damping ratio of the system has been seen to increase significantly as the pore water pressure increases. At full liquefaction, damping ratios higher than 20% are possible (see Figure 32).

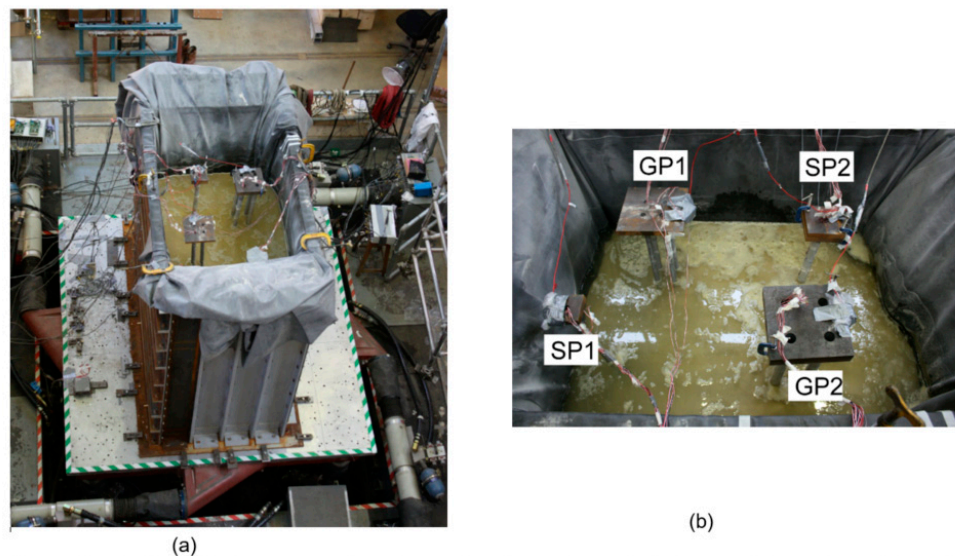


**Figure 31.** Shaking table tests on small-scale models of monopile- and pile-supported structures for the jacket: (a) geotechnical model container and shaking table; (b) model tests representing monopile-supported structures (SP1 and SP2) and  $2 \times 2$  pile-supported jacket.

From Figure 32, it can be seen that the values of frequency and damping are determined at discrete intervals during tests. An alternative method to obtain a continuous variation of frequency is to use the wavelet method [56]. The wavelet transform was introduced by the French geophysical engineer Jean Morlet to study wave propagation through soil deposits [50]. The method can be seen as an adjustable window Fourier spectral analysis in which an arbitrary signal  $x(t)$  is decomposed into a series of functions by dilation and translation of a basis function  $\psi(t)$ , known as the “mother wavelet”. As shown in Figure 33 (left), high-frequency components are reproduced by compressed mother wavelets, with

dilation parameter in the range  $0 < |a| \ll 1$ . Lower frequencies are obtained by dilated mother wavelets, with  $|a| \gg 1$ .

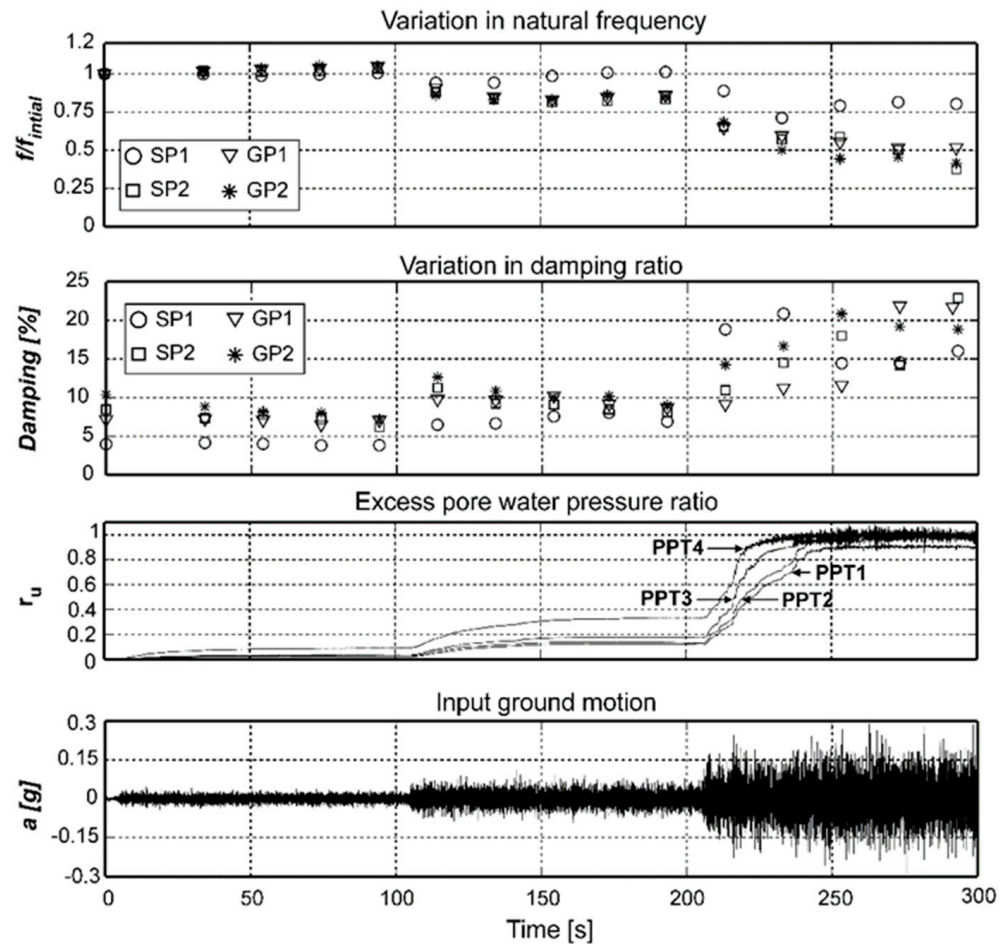


Figure 32. Typical results from shaking table tests carried out on monopile-supported structures (models labelled SP1 and SP2) and  $2 \times 2$  pile-supported structures (models labelled GP1 and GP2).

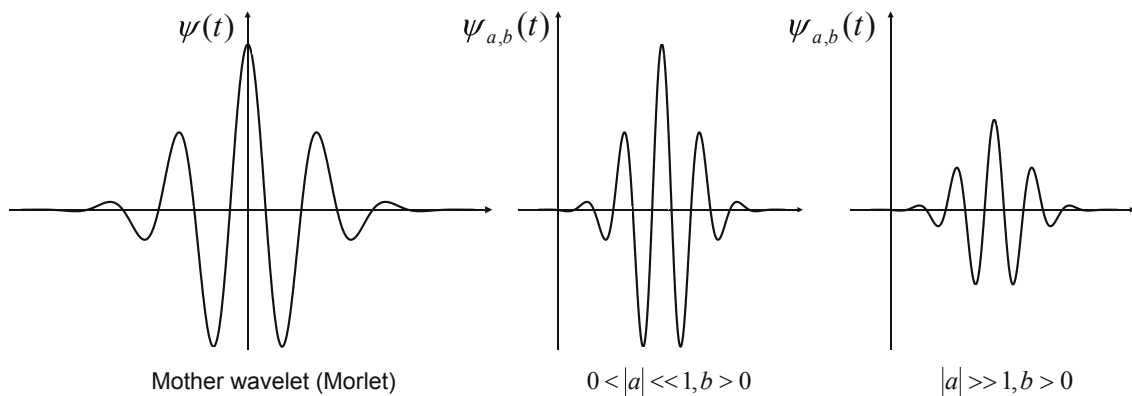
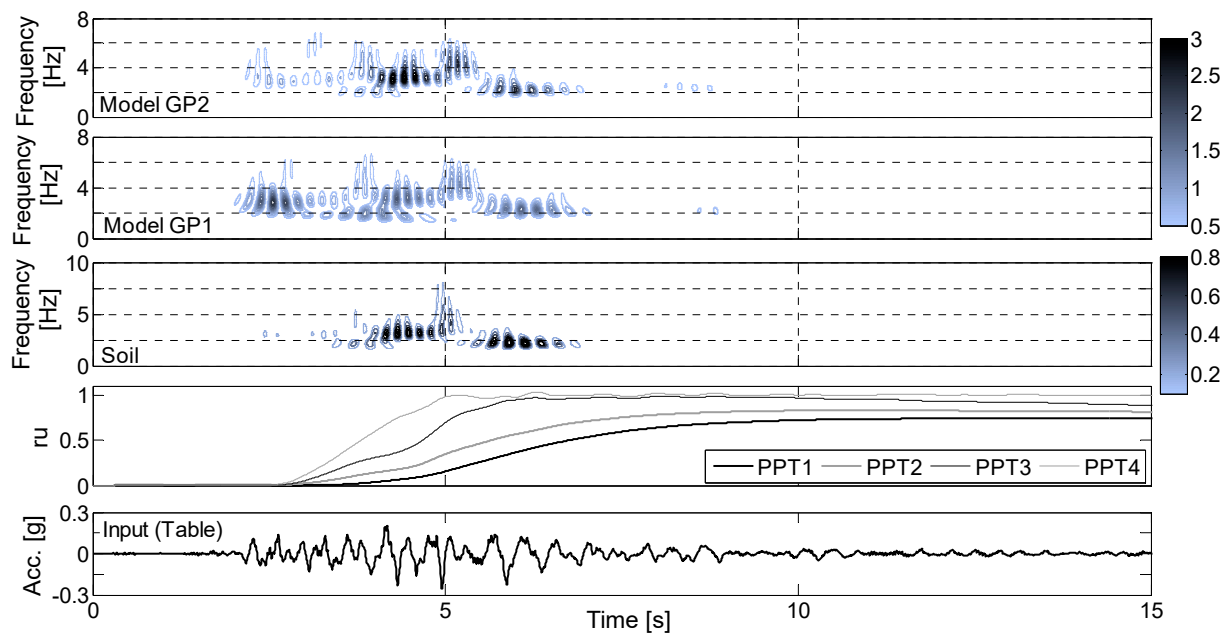


Figure 33. Qualitative representation of an example of the mother wavelet (left) and corresponding compressed (middle) and dilated versions of the mother wavelet (right).

Results from the wavelet transform are normally plotted by means of spectrograms, such as one shown in Figure 34.



**Figure 34.** Spectrograms obtained from structural and soil responses. Time histories of input acceleration and excess pore pressure ratios are also given at the bottom of the figure.

## 7. Scaling the Test Results

In this section, two examples are taken to provide insights into scaling up the tests.

### Example 1: Physical Modelling of asymmetric foundations.

For a complex multiple interaction problem such as that of offshore wind turbines, it is advisable to understand the governing physics from the scaled model tests and apply this understanding to solve the problem in hand. The proposed physical modelling framework for the prediction of the prototype response is schematically illustrated in Figure 35, whereby the asymmetric tripod is chosen. Scaled model tests showed that the system, due to its asymmetric shape and configuration, has two modes of vibration [25]. It is, therefore, necessary to alter the system so that the system has the same stiffness in two orthogonal directions. A second important point relates to the vertical stiffness required of the foundation so that rocking modes are avoided, and flexible modes of tower govern. This requires soil testing and numerical analysis. Readers are referred to [57,58] and Chapter 6 of Bhattacharya [2] for further details on how the scaling results from the small-scale models can be used to predict the response of the real prototype. The example shows the understanding can be scaled, and parametric studies can lead to different design choices.

### Example 2: Physical modelling for the seismic design of piled foundations in liquefiable soils

The application of the framework illustrated in Figure 35 can also be used to study the liquefaction-related issues for piled foundations. These are briefly summarized below.

- (a) The understanding of pile–liquefied soil interaction was understood from both shaking table tests (see Figure 31 for the setup at 1–g) and centrifuge tests. In both experiments, results showed that the liquefied soil offers negligible support to a vibrating pile and the damping of the whole system increases when the soil is liquefied.
- (b) Once a certain response is observed, the question is how the understanding and findings from the scaled model tests can inform the design method? A possible answer is to use a numerical model that captures the main mechanisms (e.g., reduction of soil strength and stiffness of the liquefied soil) whose input parameters are calibrated based on the experimental results. Different numerical models can be used; however, for the analysis of laterally loaded piles, it may be convenient to use the “beam on



nonlinear Winkler foundation” approach in which the soil–structure interaction is modelled by means of springs, which are defined in terms of  $p$ – $y$  relationships (see Figure 36). This approach is discussed in more detail below. For the case of liquefied soil, experiments at both normal gravity and multiples of gravity (centrifuge) suggest that the  $p$ – $y$  curve has an upward concave shape with an initial flat part (see Figure 37). It is important that the numerical model adopted in the analysis is consistent with the behaviour observed in the experimental studies.

- (c) How can the modeler develop  $p$ – $y$  curves that are consistent with the experimental results? This can be carried out by linking results from element tests (triaxial, simple shear) to results from small-scale model tests carried out either at  $1 \times g$  or in the centrifuge. The readers are referred to [59] for more details on the derivation of the  $p$ – $y$  curves for liquefiable soils shown in Figures 36 and 37.

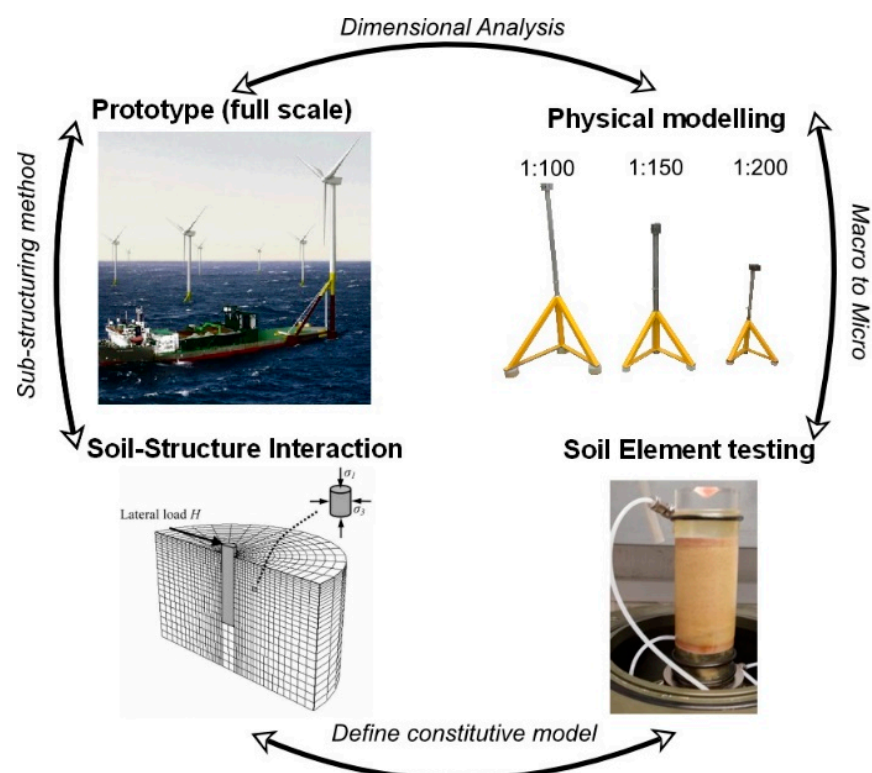
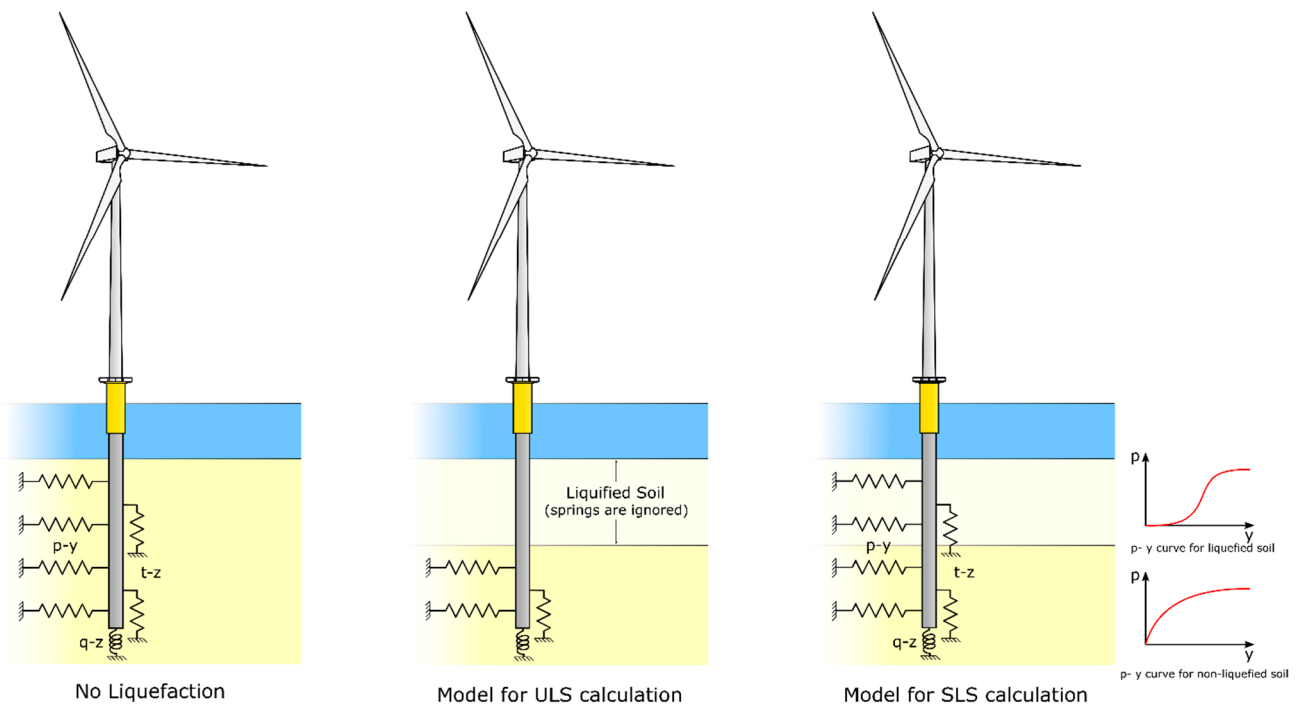


Figure 35. Physical modelling framework for the analysis of foundations.

To model laterally loaded piles, practicing engineers often use a simplified method normally referred to as the “beam on nonlinear Winkler foundation” (BNWF) [60,61]. This method is based on the hypothesis that the soil reaction exerted by the soil at a given depth on the pile shaft is proportional to the relative pile–soil lateral deflection; see Figure 36.

According to the BNWF method, the pile is modelled by means of consecutive beam–column elements, whereas the lateral pile–soil interaction is analyzed through non-linear springs that are attached to nodal points between two consecutive elements. Each spring can be defined by means of a non-linear relationship between the soil reaction (per unit length of the pile),  $p$ , and the corresponding relative soil–pile horizontal displacement,  $y$ . The coefficient of proportionality between  $p$  and  $y$  is referred to as modulus of subgrade reaction  $k$ , with a dimension of pressure divided by length. This relationship is normally known as the  $p$ – $y$  curve or reaction curve. Despite the limitation inherent in the discrete nature of the method, BNWF is extensively used in practice due to its mathematical convenience and ability to incorporate non-linearity of the soil and ground stratification.



**Figure 36.** Winkler approach for the simulation of soil–structure interaction. Each spring is defined by a non-linear spring known as  $p$ – $y$ , whose shape depends on the strength and stiffness of the material.

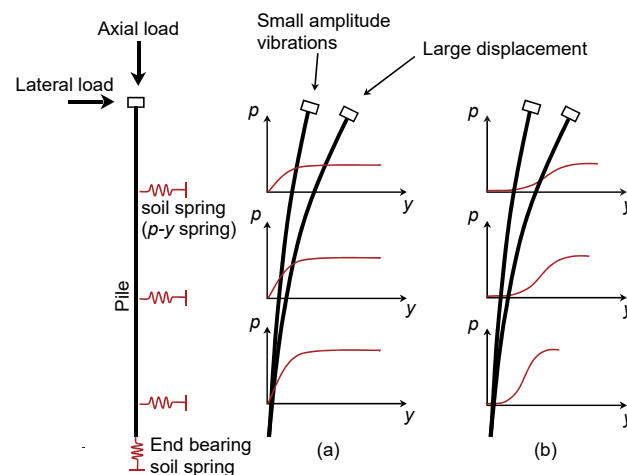


**Figure 37.** Schematic of soil–structure interaction in piled foundation depending on the shape of the  $p$ – $y$  curve: (a)  $p$ – $y$  curves from the  $p$ -multiplier approach; (b) proposed strain-hardening  $p$ – $y$  curves.

The validity of the BNWF approach is based on the assumed similarity between two mechanical system responses:

- (d) Load–deformation response of the pile, which takes into account the overall macro behavior of the soil–pile system.
- (e) Stress–strain response of the adjacent soil being sheared as the pile moves laterally. In theory, the transformation from micro to macro can be made by applying appropriate scaling factors that convert stress into equivalent soil reaction,  $p$ , and strain in equivalent relative pile–soil displacement. The scaling factors can be derived from the so-called “Mobilizable Strength Design” (MSD) method [62–64]. In routine practice, however,  $p$ – $y$  curves are constructed by means of empirical relationships, which were developed during the 1970s and 1980s based on a relatively limited number of full-scale tests carried out on small-diameter steel piles [65–69].

For liquefied soils, the  $p$ - $y$  curve presents an upward concavity with an s-shape that is consistent with the very low stiffness and strength offered by the liquefied soil and its tendency to dilate upon shearing. Figure 37 illustrates the effect of different shapes of  $p$ - $y$  curves on the seismic response of offshore wind turbines supported on a monopile. Starting from the concave-downward  $p$ - $y$  curve illustrated in Figure 37a, it can be noted that when the lateral displacement is relatively small, the soil–pile interaction depends on the initial stiffness of the reaction curve. For large displacement, however, the response is influenced by the ultimate value of the soil reaction rather than foundation stiffness. Alternatively, if the shape of the  $p$ - $y$  curve is concave-upward as in Figure 37b, the response of the pile is highly non-linear and exhibits practically zero stiffness at small displacements. Moreover, as a result of the limited resistance offered by the liquefied soil, the pile behaves as an unsupported column, which may be prone to buckling instability under large axial loads and the presence of geometrical imperfections.

Dash [70] proposed a method to construct the  $p$ - $y$  curves from a simplified stress–strain model proposed by [30]. The model required three main parameters, i.e., take-off strain  $\gamma_{to}$ , initial shear modulus,  $G_1$ , and shear modulus at large strains,  $G_2$  (see Figure 38). The advantage of this model is two-fold. First, the proposed stress–strain model requires parameters that can be conveniently determined by means of conventional element tests, such as triaxial and simple shear tests. Second, the stress–strain relationship is consistent with the strain-hardening behaviour of liquefied soils as observed in both element and physical model tests. The proposed stress–strain relationships are subsequently used to construct a novel family of  $p$ - $y$  curves for liquefiable soils. This involves scaling of stress and strain into compatible soil reaction  $p$  and pile deflection  $y$ , respectively. The proposed  $p$ - $y$  curves are finally compared with those back-calculated from centrifuge model tests.

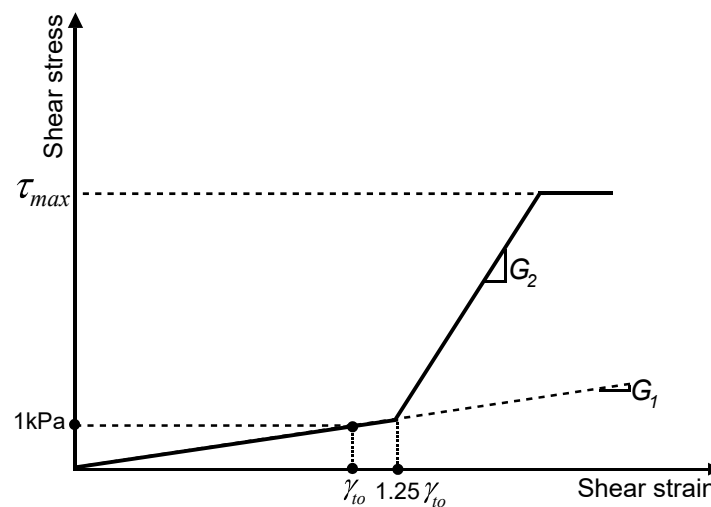
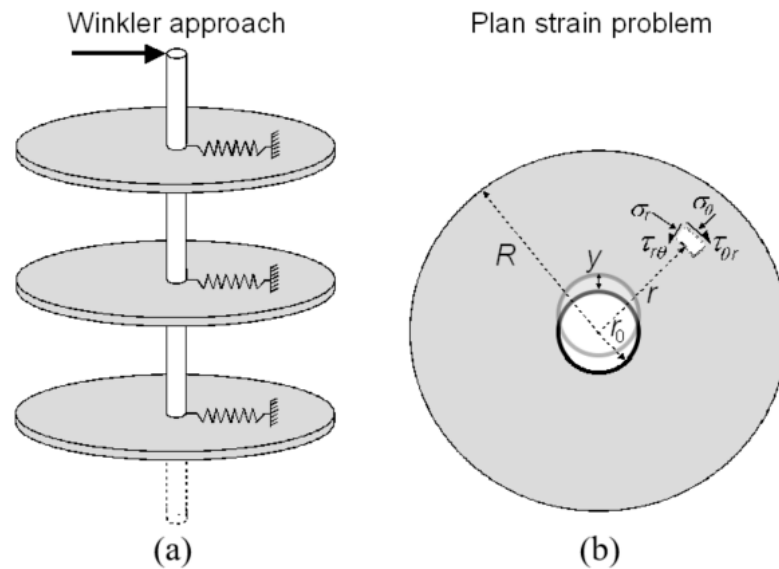


Figure 38. Monotonic stress–strain curve for liquefied soil.

The method for the construction of  $p$ - $y$  curves from stress–strain curves relies on the similarity between load–deflection characteristics of the pile and the mechanical behavior of the deforming soil (see Figure 39). This involves scaling of stress and strain into compatible soil reaction,  $p$  and pile deflection,  $y$ , respectively. It is assumed that plane strain conditions are established around the pile at any depth. As a result, soil adjacent to the foundation is expected to flow around the pile from front to back. Although such an assumption is acceptable for liquefied soils, the same may not be valid prior to the onset of liquefaction when wedge type failure is likely to occur, particularly at shallow depths. In accordance with the postulated collapse mechanism, the soil–structure interaction problem can be treated as a set of decoupled plane strain problems. As shown in Figure 39, each problem consists of a disc representing the soil, with outer radius  $R$ , and a smaller rigid disc, with outer radius  $r_0$ , which represents the pile moving laterally in the deforming soil. The soil is

assumed to adhere perfectly to the pile. It should be emphasized that the conceptualized problem is analogous to the plane strain problem employed in plasticity theory for the evaluation of the undrained lateral capacity of a cylinder moving through an infinite medium [71].



**Figure 39.** Schematic representation of idealized decoupled plane strain problem for studying soil–structure interaction: (a) modelling of laterally loaded pile according to the Winkler approach; (b) plane strain problem at a given depth.

Following Osman and Bolton (2005), the soil resistance  $p$  developed at a mobilized stress  $\tau_{mob}$  is given by:

$$p = N_s \tau_{mob} D \tag{1}$$

in which  $N_s$  is a scaling factor for stress. The mobilized shear stress  $\tau_{mob}$  can be related to an average mobilized engineering shear strain  $\gamma_{s,mob}$ , defined as the spatial average of the shear strain  $\gamma_s$  in the entire volume of the deforming medium. Introducing the scaling factor for strain,  $M_s$ , the average mobilized engineering shear strain is given by:

$$\gamma_{s,mob} = \frac{\int_V \gamma_s \cdot dV}{\int_V dV} = M_s \frac{y}{D} \tag{2}$$

It is noted that the engineering shear strain  $\gamma_s$  is defined as the difference between major  $\epsilon_1$  and minor principal  $\epsilon_3$  strains:

$$\gamma_s = \epsilon_1 - \epsilon_3 \tag{3}$$

If the stress–strain curve to be converted into a  $p$ – $y$  curve is obtained from triaxial compression tests, the major and minor principal strains correspond to the axial  $\epsilon_a$  and radial  $\epsilon_r$  strains, respectively. Considering that liquefaction occurs in undrained conditions, the engineering shear strain  $\gamma_s$  can be expressed in terms of axial strain  $\epsilon_a$ , such that:

$$\gamma_s = \epsilon_1 - \epsilon_3 = \epsilon_a - \epsilon_r = 1.5\epsilon_a \tag{4}$$

Because the loading is axisymmetric, and neglecting end-effects and possible problems associated with the initial anisotropy of the sample, the major  $\sigma_1$  and minor  $\sigma_3$  princi-

pal stresses correspond to the axial  $\sigma_a$  and radial  $\sigma_r$ , respectively. In this condition, the mobilized stress  $\tau_{mob}$  simplifies to:

$$\tau_{mob} = \frac{\sigma_1 - \sigma_3}{2} = \frac{\sigma_a - \sigma_r}{2} \tag{5}$$

*Derivation of Scaling Parameters*

Drawing on the concept of the mobilisable strength design (MSD) method (Bolton and Powrie, 1988; Osman and Bolton, 2005), and its extension (EMSD) by Klar and Osman (2008), which differs from the former in having a deformation mechanism that changes throughout the loading sequence, an energy-based approach is used to obtain the scaling factors  $N_s$  and  $M_s$ . Assuming that the soil–pile system is initially in equilibrium, the rate of input work  $\dot{W}$  done by the moving disc—representing the pile—is given by:

$$\dot{W} = p\dot{y} \tag{6}$$

in which  $\dot{y}$  denotes the increment in lateral displacement, and  $p$  the resulting soil reaction (per unit length of the pile). The rate of dissipation of energy  $\dot{E}$  within the deforming soil mass, with volume  $V$ , is given by:

$$\dot{E} = \int_V (\sigma_1 \dot{\epsilon}_1 + \sigma_3 \dot{\epsilon}_3) dV \tag{7}$$

The hypothesis of incompressibility implies that major and minor principal strain rates are equal and opposite:  $\dot{\epsilon}_1 = -\dot{\epsilon}_3$ . The rate of dissipation of energy  $\dot{E}$  is expressed as a function of mobilized parameters by:

$$\dot{E} = \int_V (\sigma_1 - \sigma_3) \dot{\epsilon}_1 dV = 2 \int_V \tau_{mob} \dot{\epsilon}_1 dV = \int_V \tau_{mob} \dot{\gamma}_{s,mob} dV \tag{8}$$

The scaling factor for stress  $N_s$  is estimated by equating the rate of dissipation of internal energy within the deforming soil to work done by the external load, namely,  $\dot{E} = \dot{W}$ . In seeking an upper bound solution to the problem,  $N_s$  is sought, which minimizes the internal work:

$$N_s = \frac{\min \left[ \int_V \tau_{mob} \dot{\gamma}_{s,mob} dV \right]}{\tau_{mob} D \dot{y}} \tag{9}$$

The upper bound calculation required an incremental numerical procedure in which the soil can be modelled in a FE (see Figure 40). The incremental displacement  $\dot{y}$  was applied to the inner boundary of the soil, whereas the exterior boundary was fixed (see Figure 40). The deforming medium can be modelled using the simplified strain-hardening shown in Figure 41b. Typical results from this type of analysis can be found in Figure 41. The optimal upper bound solution requires the evaluation of the lowest possible value of  $\dot{E}$ , at each incremental displacement and different radial distances  $R$ . The proposed scaling procedure of stress–strain into compatible  $p$ – $y$  curves is schematically depicted in Figure 41a.

The proposed method of scaling element results into  $p$ – $y$  curves that account for macro soil–structure interaction of piled foundations was validated by [35] by means of centrifuge tests. The tests considered in this paper were carried out in the centrifuge facility of Shimizu Corporation (Japan). Detailed information on the centrifuge facility can be found in [72]. The experimental setup used in the centrifuge tests is shown in Figure 42. The reader is referred to [35] for more details regarding the tests.

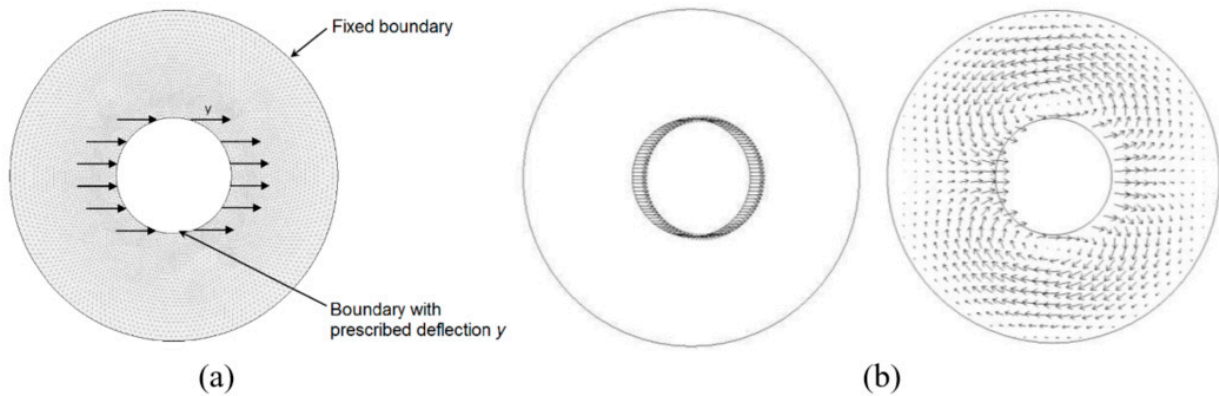


**Figure 40.** Numerical model used for evaluation of scaling factors  $M_s$  and  $N_s$ : (a) mesh used in FE model; (b) typical deformation mechanism.

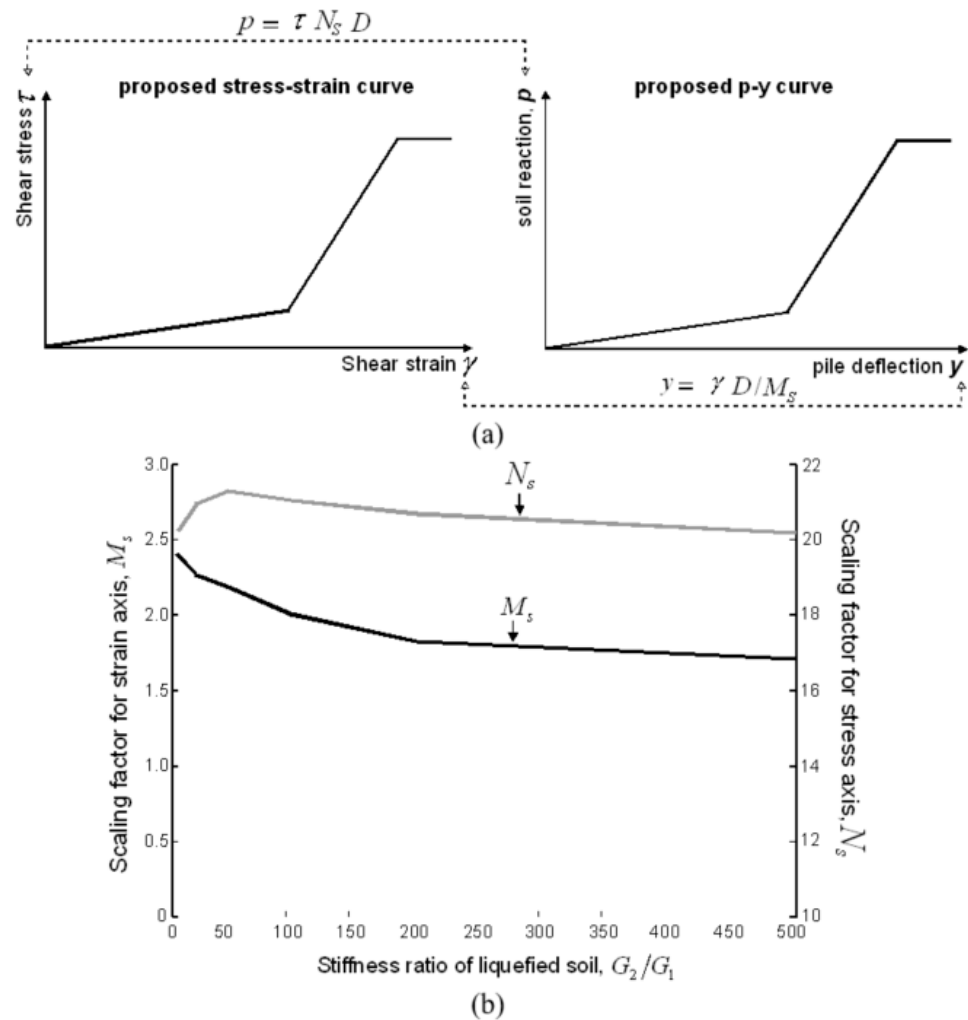


**Figure 41.** (a) Proposed scaling approach for derivation of  $p$ - $y$  curves from the stress-strain curve; (b) computed scaling factors  $M_s$  and  $N_s$  for different stiffness ratios  $G_2/G_1$ .

Derivation of  $p$ - $y$  curves from test data

The derivation of the  $p$ - $y$  curve involved four major steps, summarised as follows:

- (a) Double integration of soil acceleration to compute soil displacement  $y_s$ . The acceleration can be measured by accelerometers.
- (b) Double integration of bending moment along the pile to obtain pile deflection  $y_p$ . The bending moment can be obtained from strain-gauge pairs installed at different elevations along the foundation.
- (c) The relative pile–soil displacement  $y$  can be computed as the difference  $y_p - y_s$ ;
- (d) Double differentiation of bending moment along the pile to obtain soil reaction  $p$ .

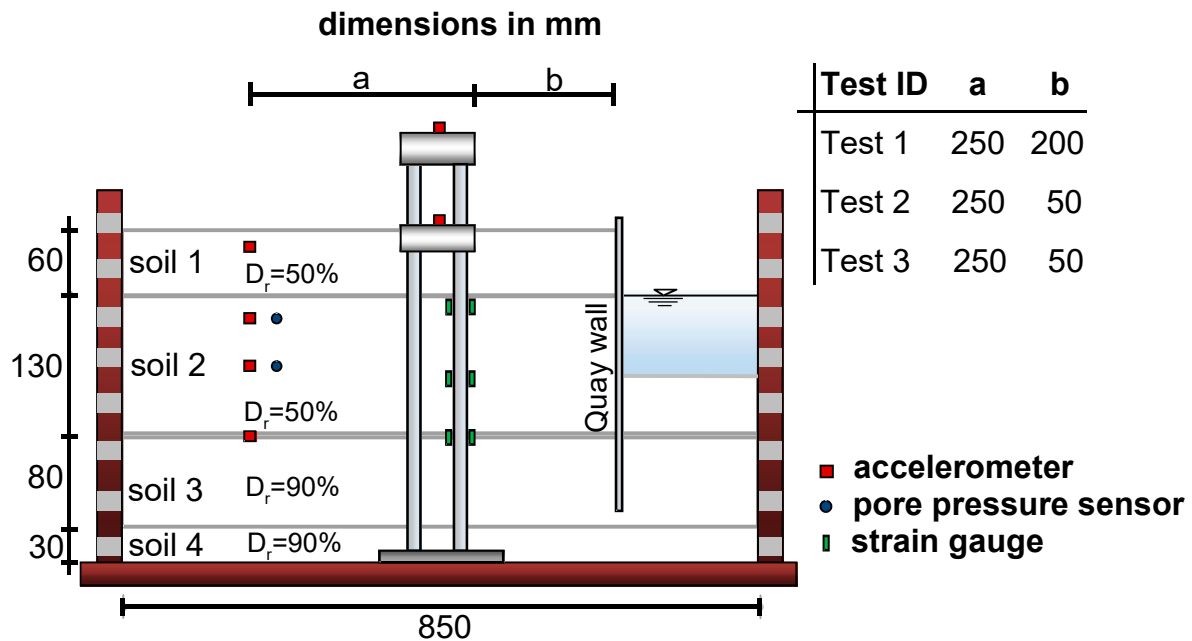


Figure 42. Test setup and instrumental layout used in centrifuge tests.

Because the numerical operations of integration and differentiation are sensitive to low frequency and high-frequency noise, a band-pass Butterworth filter needs to be applied to all records before signal processing. Furthermore, because the computed bending moments are normally known only at discrete locations, a cubic spline interpolation function is used to obtain a continuous bending curve along with the instrumented pile. An example of back-calculated  $p$ – $y$  curves is illustrated in Figure 43, in which the soil resistance  $p$  is normalised by the effective stress  $\sigma'_v$  and pile diameter  $D$ , and the displacement  $y$  is normalised by the pile diameter  $D$ . Based on the back-calculated  $p$ – $y$  curves, the following conclusions may be drawn:

- (e) Figure 43 displays  $p$ – $y$  curves relative to three depths within the liquefiable layer (i.e., soil layer 2 in Figure 43). It can be seen that the back-calculated  $p$ – $y$  curves exhibited practically zero stiffness at small deflection. The implication of using  $p$ – $y$  curves having different shapes was previously discussed through the schematic representation in Figure 37.
- (f) Figure 44 compares the back-calculated  $p$ – $y$  curves with those computed from the proposed and  $p$ -multiplier methods. It can be observed that the back-calculated  $p$ – $y$  curves exhibit low stiffness at small lateral displacement, and increasing stiffness and lateral resistance with increasing  $y$ . This strain-hardening behaviour is better captured by the proposed  $p$ – $y$  curves than the routine method, which clearly overestimates the initial foundation stiffness.

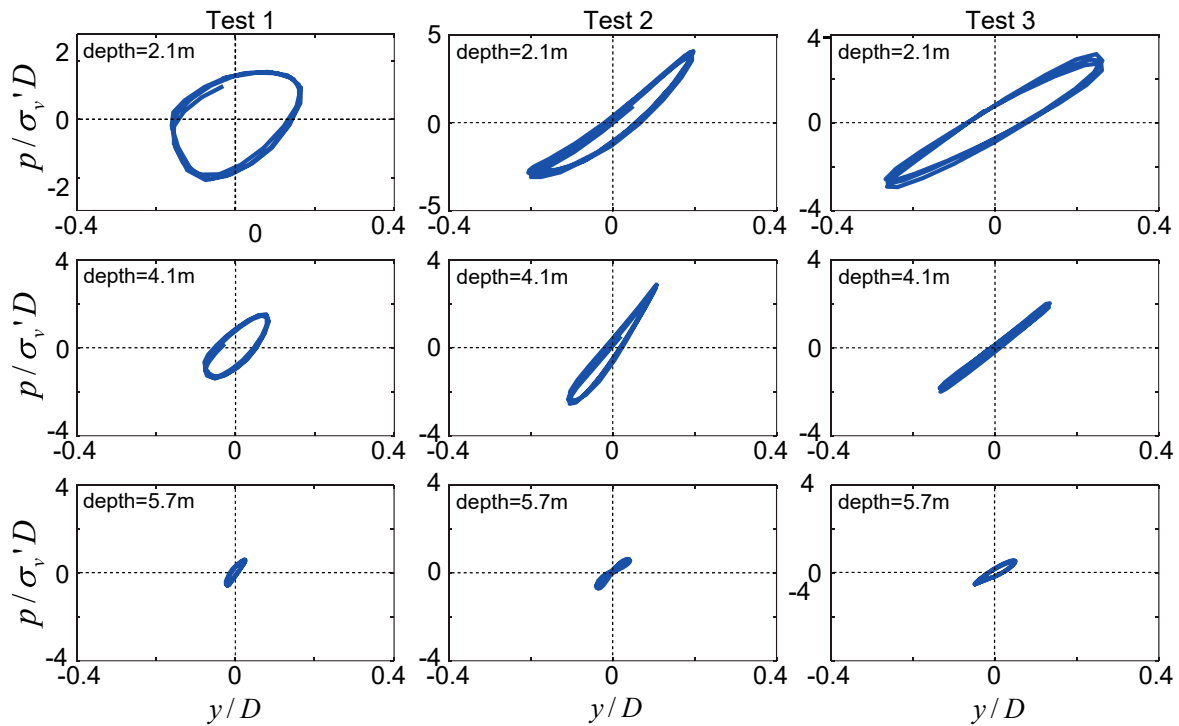


Figure 43. Back-calculated  $p$ - $y$  curves from centrifuge tests.

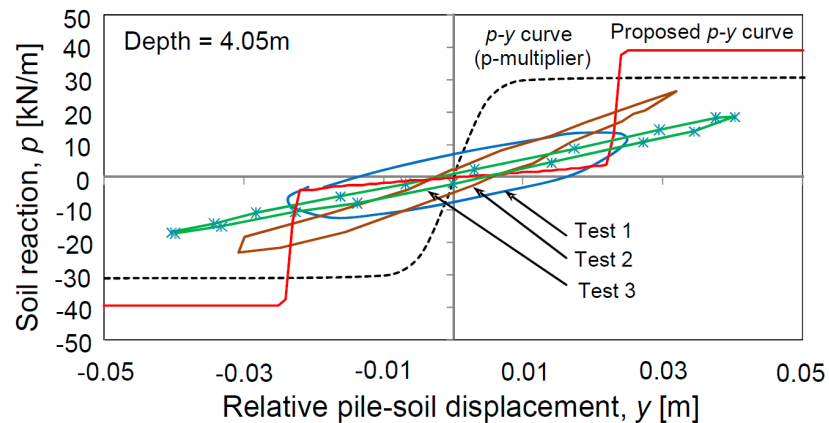


Figure 44. Comparison between  $p$ - $y$  curves back-calculated from centrifuge tests and  $p$ - $y$  curves constructed according to the proposed method and the  $p$ -multiplier approach for various methods.

### 8. Discussion and Conclusions

Offshore wind turbines are relatively new structures that are being installed in large numbers in complex ground conditions and in challenging environmental conditions. This leads to the use of non-conventional foundations for which guidelines do not yet exist. In these cases, efficacy studies must be carried out to assess the Technology Readiness Level (TRL), and the applicability must be determined. Scaled model tests are carried out as a part of such a study, and one of the intellectual aspects is the scaling laws, i.e., how to scale test results to predict the prototype. This paper showed that the engineering solution for a particular problem is to iterate to converge to the best scaling laws. This approach requires multi-scale testing, state-of-the-art numerical FEA, and insightful reduced-order mechanics/physics models. Predictions require a fusion of (i) reduced-order models and FEA models, (ii) small-scale tests (centrifuge, shake table tests at normal gravity, material element testing), and (iii) full-field monitoring observations. Different types of scaled physical modelling, such as geotechnical centrifuge modelling under enhanced



pseudo-gravity and  $1 \times g$  scaled modelling under Earth's gravity, are discussed. Example applications of TRL studies for a range of foundations are illustrated.

**Author Contributions:** Conceptualization, S.B. and D.L.; methodology, S.B., D.L., N.A., G.P., S.A. (Sondipon Adhikari), Y.W., L.C.; resources, V.P., S.J., M.A., S.A. (Sadra Amani), A.A., W.L., J.M. and N.V.; writing—original draft preparation, S.B. and M.A.; writing—review and editing, V.P., D.L.; visualization, M.A., S.A. (Sadra Amani), D.L. and J.M. All authors have read and agreed to the published version of the manuscript.

**Funding:** This research received no external funding.

**Institutional Review Board Statement:** Not applicable.

**Informed Consent Statement:** Not applicable.

**Data Availability Statement:** Not applicable.

**Acknowledgments:** S. Bhattacharya would like to record appreciation for generous funding and insights into wind turbine foundation issues from the following organisations: University of Bristol and Surrey, developers Innogy, RWE, TEPSCO, Mott Macdonald, Atkins, EPSRC EP/H015345/1 EP/H015345/2. S. Bhattacharya also acknowledges the contribution of Nick Nikitas (University of Leeds) for his help during the experiments of scaled model testing using the Bristol shaking table. S. Adhikari acknowledges the support from the Marie Skłodowska-Curie Actions—European Commission: MSCA-IF-2019-890419, (SMART-UP). Vikram Pakrashi would like to acknowledge that this publication has emanated from research Science Foundation Ireland under Grant number RC2302\_2 and acknowledges the UCD Energy Institute and UCD Centre for Mechanics.

**Conflicts of Interest:** The authors declare no conflict of interest.

## References

- Pagani, M.; Garcia-Pelaez, J.; Gee, R.; Johnson, K.; Poggi, V.; Styron, R.; Weatherill, G.; Simionato, M.; Viganò, D.; Danciu, L.; et al. Global Earthquake Model (GEM): Seismic Hazard Map. Version 2018.1—December 2018. Available online: [https://www.preventionweb.net/files/65696\\_hazardmapcompressed.pdf](https://www.preventionweb.net/files/65696_hazardmapcompressed.pdf) (accessed on 25 January 2021).
- Bhattacharya, S. *Design of Foundations for Offshore Wind Turbines*; Wiley: Hoboken, NJ, USA, 2019.
- Bhattacharya, S.; Wang, L.; Liu, J.; Hong, Y. Civil engineering challenges associated with design of offshore wind turbines with special reference to China. In *Wind Energy Engineering*; Academic Press: Cambridge, MA, USA, 2017; pp. 243–273.
- Arany, L.; Bhattacharya, S.; Macdonald, J.; Hogan, S.J. Design of monopiles for offshore wind turbines in 10 steps. *Soil Dyn. Earthq. Eng.* **2017**, *92*, 126–152. [[CrossRef](#)]
- Arany, L.; Bhattacharya, S.; Adhikari, S.; Hogan, S.; Macdonald, J.H.G. An analytical model to predict the natural frequency of offshore wind turbines on three-spring flexible foundations using two different beam models. *Soil Dyn. Earthq. Eng.* **2015**, *74*, 40–45. [[CrossRef](#)]
- Bhattacharya, S.; Demirci, H.E.; Nikitas, G.; Prakhya, G.K.V.; Lombardi, D.; Alexander, N.A.; Aleem, M.; Amani, S.; Mylonakis, G. Physical modeling of interaction problems in geotechnical engineering. In *Modeling in Geotechnical Engineering*; Academic Press: Cambridge, MA, USA, 2021; pp. 205–256.
- O'Leary, K.; Pakrashi, V.; Kelliher, D. Optimisation of composite material tower for offshore wind turbine structures. *Renew. Energy* **2019**, *140*, 928–942. [[CrossRef](#)]
- O'Kelly-Lynch, P.; Long, C.; McAuliffe, F.D.; Murphy, J.; Pakrashi, V. Structural design implications of combining a point absorber with a wind turbine monopile for the east and west coast of Ireland. *Renew. Sustain. Energy Rev.* **2020**, *119*, 109583. [[CrossRef](#)]
- O'Donnell, D.; Srbinovsky, B.; Murphy, J.; Popovici, E.; Pakrashi, V. Sensor Measurement Strategies for Monitoring Offshore Wind and Wave Energy Devices. *J. Phys. Conf. Ser.* **2015**, *628*, 012117. [[CrossRef](#)]
- O'Donnell, D.; Murphy, J.; Pakrashi, V. Damage Monitoring of a Catenary Moored Spar Platform for Renewable Energy Devices. *Energies* **2020**, *13*, 3631. [[CrossRef](#)]
- Leimeister, M.; Collu, M.; Kolios, A. A fully integrated optimization framework for designing a complex geometry offshore wind turbine spar-type floating support structure. *Wind Energy Sci. Discuss.* **2020**, *5*, 1–35. [[CrossRef](#)]
- Davidson, C.; Brown, M.J.; Cerfontaine, B.; Al-Baghdadi, T.; Knappett, J.; Brennan, A.; Augarde, C.; Coombs, W.; Wang, L.; Blake, A.; et al. Physical modelling to demonstrate the feasibility of screw piles for offshore jacket-supported wind energy structures. *Géotechnique* **2020**, 1–19. [[CrossRef](#)]
- Karimi, H.R.; Zapateiro, M.; Luo, N. Semiactive vibration control of offshore wind turbine towers with tuned liquid column dampers using H $\infty$  output feedback control. In Proceedings of the 2010 IEEE International Conference on Control Applications, Yokohama, Japan, 8–10 September 2010; pp. 2245–2249.
- Buckley, T.; Watson, P.; Cahill, P.; Jaksic, V.; Pakrashi, V. Mitigating the structural vibrations of wind turbines using tuned liquid column damper considering soil-structure interaction. *Renew. Energy* **2018**, *120*, 322–341. [[CrossRef](#)]

15. Jaksic, V.; Wright, C.S.; Murphy, J.; Afeef, C.; Ali, S.F.; Mandic, D.P.; Pakrashi, V. Dynamic response mitigation of floating wind turbine platforms using tuned liquid column dampers. *Philos. Trans. R. Soc. A Math. Phys. Eng. Sci.* **2015**, *373*, 20140079. [[CrossRef](#)]
16. Jaksic, V.; O'Shea, R.; Cahill, P.; Murphy, J.; Mandic, D.P.; Pakrashi, V. Dynamic response signatures of a scaled model platform for floating wind turbines in an ocean wave basin. *Philos. Trans. R. Soc. A Math. Phys. Eng. Sci.* **2015**, *373*, 20140078. [[CrossRef](#)] [[PubMed](#)]
17. Byrne, B.; McAdam, R.; Burd, H.; Houlsby, G.; Martin, C.; Beuckelaers, W.; Zdravkovic, L.; Taborda, D.; Potts, D.; Jardine, R.; et al. PISA: New Design Methods for Offshore Wind Turbine Monopiles. In Proceedings of the Offshore Site Investigation Geotechnics 8th International Conference Proceedings, London, UK, 12–14 September 2017; Society for Underwater Technology: London, UK, 2017; Volume 142, pp. 142–161. [[CrossRef](#)]
18. O'Donnell, D.; Murphy, J.; Pakrashi, V. Comparison of Response Amplitude Operator Curve Generation Methods for Scaled Floating Renewable Energy Platforms in Ocean Wave Basin. *ASME Lett. Dyn. Syst. Control* **2021**, *1*, 021012. [[CrossRef](#)]
19. O'Byrne, M.; Schoefs, F.; Pakrashi, V.; Ghosh, B. An underwater lighting and turbidity image repository for analysing the performance of image-based non-destructive techniques. *J. Struct. Infrastruct. Eng.* **2018**, *14*, 104–123. [[CrossRef](#)]
20. Benregui, P.; Kelly, J.; Pakrashi, V.; Murphy, J. Wave-to-Wire model development and validation for Two OWC type wave energy converters. *Energies* **2019**, *12*, 3977. [[CrossRef](#)]
21. Benregui, P.; Pakrashi, V.; Murphy, J. Assessment of Primary Energy Conversion of a Closed-Circuit OWC Wave Energy Converter. *Energies* **2019**, *12*, 1962. [[CrossRef](#)]
22. Malekjafarian, A.; Jalilvand, S.; Doherty, P.; Igoe, D. Foundation damping for monopile supported offshore wind turbines: A review. *Mar. Struct.* **2021**, *77*, 102937. [[CrossRef](#)]
23. Adhikari, S.; Bhattacharya, S. A general frequency adaptive framework for damped response analysis of wind turbines. *Soil Dyn. Earthq. Eng.* **2021**, *143*, 106605. [[CrossRef](#)]
24. Bhattacharya, S.; Lombardi, D.; Wood, D.M. Similitude relationships for physical modelling of mono-pile-supported offshore wind turbines. *Int. J. Phys. Model. Geotech.* **2011**, *11*, 58–68.
25. Bhattacharya, S.; Nikitas, N.; Garnsey, J.; Alexander, N.; Cox, J.; Lombardi, D.; Wood, D.M.; Nash, D. Observed dynamic soil–structure interaction in scale testing of offshore wind turbine foundations. *Soil Dyn. Earthq. Eng.* **2013**, *54*, 47–60. [[CrossRef](#)]
26. Hall, F.; Lombardi, D.; Bhattacharya, S. Identification of transient vibration characteristics of pile-group models during liquefaction using wavelet transform. *Eng. Struct.* **2018**, *171*, 712–729. [[CrossRef](#)]
27. Adhikari, S.; Bhattacharya, S. Vibrations of wind-turbines considering soil-structure interaction. *Wind. Struct.* **2011**, *14*, 85–112. [[CrossRef](#)]
28. Jalbi, S.; Arany, L.; Salem, A.; Cui, L.; Bhattacharya, S. A method to predict the cyclic loading profiles (one-way or two-way) for monopile supported offshore wind turbines. *Mar. Struct.* **2019**, *63*, 65–83. [[CrossRef](#)]
29. Jalbi, S.; Bhattacharya, S. A comparison between advanced and simplified methods to predict the natural frequency of offshore wind turbines incorporating soil-structure interaction. *Coast. Struct.* **2019**, *2019*, 904–912.
30. Lombardi, D.; Bhattacharya, S.; Wood, D.M. Dynamic soil–structure interaction of monopile supported wind turbines in cohesive soil. *Soil Dyn. Earthq. Eng.* **2013**, *49*, 165–180. [[CrossRef](#)]
31. Nikitas, G.; Vimalan, N.J.; Bhattacharya, S. An innovative cyclic loading device to study long term performance of offshore wind turbines. *Soil Dyn. Earthq. Eng.* **2016**, *82*, 154–160. [[CrossRef](#)]
32. Yu, L.-Q.; Wang, L.-Z.; Guo, Z.; Bhattacharya, S.; Nikitas, G.; Li, L.-L.; Xing, Y.-L. Long-term dynamic behavior of monopile supported offshore wind turbines in sand. *Theor. Appl. Mech. Lett.* **2015**, *5*, 80–84. [[CrossRef](#)]
33. Guo, Z.; Yu, L.; Wang, L.; Bhattacharya, S.; Nikitas, G.; Xing, Y. Model Tests on the Long-Term Dynamic Performance of Offshore Wind Turbines Founded on Monopiles in Sand. *J. Offshore Mech. Arct. Eng.* **2015**, *137*, 041902. [[CrossRef](#)]
34. Xu, Y.; Nikitas, G.; Zhang, T.; Han, Q.; Chryssanthopoulos, M.; Bhattacharya, S.; Wang, Y. Support condition monitoring of offshore wind turbines using model updating techniques. *Struct. Health Monit.* **2020**, *19*, 1017–1031. [[CrossRef](#)]
35. Lombardi, D.; Bhattacharya, S. Evaluation of seismic performance of pile-supported models in liquefiable soils. *Earthq. Eng. Struct. Dyn.* **2016**, *45*, 1019–1038. [[CrossRef](#)]
36. Lombardi, D. Dynamics of Pile-Supported Structures in Seismically Liquefiable Soils. Ph.D. Thesis, University of Bristol, Bristol, UK, 2014.
37. Lombardi, D.; Bhattacharya, S.; Hyodo, M.; Kaneko, T. Undrained behaviour of two silica sands and practical implications for modelling SSI in liquefiable soils. *Soil Dyn. Earthq. Eng.* **2014**, *66*, 293–304. [[CrossRef](#)]
38. Jaksic, V.; Wright, C.; Mandic, D.P.; Murphy, J.; Pakrashi, V. A delay vector variance based marker for an output-only assessment of structural changes in tension leg platforms. *J. Phys. Conf. Ser.* **2015**, *628*, 012059. [[CrossRef](#)]
39. Arany, L.; Bhattacharya, S. Simplified load estimation and sizing of suction anchors for spar buoy type floating offshore wind turbines. *Ocean Eng.* **2018**, *159*, 348–357. [[CrossRef](#)]
40. Welch, P. The use of fast Fourier transform for the estimation of power spectra: A method based on time averaging over short, modified periodograms. *IEEE Trans. Audio Electroacoust.* **1967**, *15*, 70–73. [[CrossRef](#)]
41. Bhattacharya, S.; Cox, J.A.; Lombardi, D.; Wood, D.M. Dynamics of offshore wind turbines supported on two foundations. *Proc. Inst. Civ. Eng. Geotech. Eng.* **2013**, *166*, 159–169. [[CrossRef](#)]

42. Cox, J.A.; O'Loughlin, C.; Cassidy, M.; Bhattacharya, S.; Gaudin, C.; Bienen, B. Centrifuge study on the cyclic performance of caissons in sand. *Int. J. Phys. Model. Geotech.* **2014**, *14*, 99–115. [[CrossRef](#)]
43. Bhattacharya, S.; Lombardi, D.; Dihoru, L.; Dietz, M.S.; Crewe, A.J.; Taylor, C.A. Model container design for soil-structure interaction studies. In *Role of Seismic Testing Facilities in Performance-Based Earthquake Engineering*; Springer: Dordrecht, The Netherlands, 2012; pp. 135–158.
44. Lombardi, D.; Bhattacharya, S.; Scarpa, F.; Bianchi, M. Dynamic response of a geotechnical rigid model container with absorbing boundaries. *Soil Dyn. Earthq. Eng.* **2015**, *69*, 46–56. [[CrossRef](#)]
45. Kolsky, H. *Stress Waves in Solids*; Clarendon Press: Oxford, UK, 1953.
46. Cohen, L. *Time-Frequency Analysis*; Prentice-Hall: Englewood Cliffs, NJ, USA, 1995.
47. Simpson, J.J. Oceanographic and atmospheric applications of spatial statistics and digital image analysis. In *Spatial Statistics and Digital Image Analysis*; National Academy Press: Washington, DC, USA, 1991.
48. Huang, N.E.; Shen, Z.; Long, S.R.; Wu, M.C.; Shih, H.H.; Zheng, Q.; Yen, N.C.; Tung, C.C.; Liu, H.H. The empirical mode decomposition and the Hilbert spectrum for non-linear and non-stationary time series analysis. *Philos. Trans. R. Soc. A Math. Phys. Eng. Sci.* **1991**, *454*, 903–995. [[CrossRef](#)]
49. Huang, N.E.; Wu, Z. A review on Hilbert-Huang transform: Method and its applications to geophysical studies. *Rev. Geophys.* **2008**, *46*, 1–23. [[CrossRef](#)]
50. Morlet, J.; Arens, G.; Fourgeau, E.; Glard, D. Wave propagation and sampling theory—Part I: Complex signal and scattering in multilayered media. *Geophysics* **1982**, *47*, 203–221. [[CrossRef](#)]
51. Gurley, K.; Kareem, A. Applications of wavelet transforms in earthquake, wind and ocean engineering. *Eng. Struct.* **1999**, *21*, 149–167.
52. Chakraborty, A.; Okaya, D. Frequency-time decomposition of seismic data using wavelet-based methods. *Geophysics* **1995**, *60*, 1906–1916. [[CrossRef](#)]
53. Basu, B.; Gupta, V.K. Stochastic seismic response of single-degree-of-freedom systems through wavelets. *Eng. Struct.* **2000**, *22*, 1714–1722. [[CrossRef](#)]
54. Lombardi, D.; Bhattacharya, S. Modal analysis of pile-supported structures during seismic liquefaction. *Earthq. Eng. Struct. Dyn.* **2014**, *43*, 119–138. [[CrossRef](#)]
55. Lombardi, D. *Dynamics of Offshore Wind Turbines*; University of Bristol: Bristol, UK, 2010.
56. Iyama, J.; Kuwamura, H. Application of wavelets to analysis and simulation of earthquake motions. *Earthq. Eng. Struct. Dyn.* **1999**, *28*, 255–272. [[CrossRef](#)]
57. Jalbi, S.; Nikitas, G.; Bhattacharya, S.; Alexander, N. Dynamic design considerations for offshore wind turbine jackets supported on multiple foundations. *Mar. Struct.* **2019**, *67*, 102631. [[CrossRef](#)]
58. Jalbi, S.; Bhattacharya, S. Minimum foundation size and spacing for jacket supported offshore wind turbines considering dynamic design criteria. *Soil Dyn. Earthq. Eng.* **2019**, *123*, 193–204. [[CrossRef](#)]
59. Dash, S.; Rouholamin, M.; Lombardi, D.; Bhattacharya, S. A practical method for construction of p-y curves for liquefiable soils. *Soil Dyn. Earthq. Eng.* **2017**, *97*, 478–481. [[CrossRef](#)]
60. Winkler, E. Die Lehre von der Elasticitaet und Festigkeit Besonderer Rucksicht auf ihre Anwendung in der Technik fur Politechnische Schulen, Bauakademien, Ingenieure, Maschinenbauer, Architekten, etc. 1867. Available online: [https://archive.org/details/bub\\_gb\\_25E5AAAACAAJ](https://archive.org/details/bub_gb_25E5AAAACAAJ) (accessed on 26 May 2021).
61. Hetényi, M. *Beams on Elastic Foundation: Theory with Applications in the Fields of Civil and Mechanical Engineering*; The University of Michigan Press: Ann Arbor, MI, USA, 1946.
62. Bouzid, D.J.; Bhattacharya, S.; Dash, S.R. Winkler Springs (p-y curves) for pile design from stress-strain of soils: FE assessment of scaling coefficients using the Mobilised Strength Design concept. *Geomech. Eng.* **2013**, *5*, 379–399. [[CrossRef](#)]
63. Bolton, M.D.; Powrie, W. Behavior of diaphragm walls in clay prior to collapse. *Géotechnique* **1988**, *38*, 167–189. [[CrossRef](#)]
64. Osman, A.S.; Bolton, M.D. A new design method for retaining walls in clay. *Can. Geotech. J.* **2004**, *41*, 451–466. [[CrossRef](#)]
65. Matlock, H. Correlation for design of laterally loaded piles in soft clay. In Proceedings of the Offshore Technology Conference, Houston, TX, USA, 21–23 April 1970; pp. 77–94.
66. Reese, L.C.; Cox, W.R.; Koop, F.D. Analysis of Laterally Loaded Piles in Sand. In Proceedings of the Offshore Technology Conference, Houston, TX, USA, 5–7 May 1974; Volume 2.
67. Reese, L.C.; Cox, W.R.; Koop, F.D. Field Testing and Analysis of Laterally Loaded Piles in Stiff Clay. In Proceedings of the Offshore Technology Conference, Houston, TX, USA, 5–7 May 1975.
68. O'Neill, M.W.; Murchison, J.M. *An Evaluation of p-y Relationships in Sands*; Report to American Petroleum Institute; University of Texas at Austin: Austin, TX, USA, 1983.
69. Aleem, M.; Demirci, H.E.; Bhattacharya, S. Lateral and Moment Resisting Capacity of Monopiles In Layered Soils. In Proceedings of the ICEESEN, Kayseri, Turkey, 19 November 2020; pp. 19–21.
70. Dash, S. Lateral Pile-Soil Interaction in Liquefiable Soils. Ph.D. Thesis, University of Oxford, Oxford, UK, 2010.
71. Randolph, M.F.; Houlsby, G.T. The limiting pressure on a circular pile loaded laterally in cohesive soil. *Géotechnique* **1984**, *34*, 613–623. [[CrossRef](#)]
72. Sato, M. A new dynamic geotechnical centrifuge and performance of shaking table tests. *Int. Conf. Cent.* **1994**, *94*, 157–162.